THE SUN AND THE HELIOSPHERE AS AN INTEGRATED SYSTEM

THE SUN AND THE HELIOSPHERE AS AN INTEGRATED SYSTEM

Edited by
GIANNINA POLETTO
INAF, Osservatorio Astrofisico di Arcetri, Firenze, Italy

STEVEN T. SUESS
NSSTC, NASA Marshall Space Flight Center, Huntsville, Alabama, USA

Kluwer Academic Publishers
Boston/Dordrecht/London

A C.I.P. Catalogue record for this book is available from the Library of Congress.

ISBN 1-4020-2830-X (HB)
ISBN 1-4020-2831-8 (e-book)

Published by Kluwer Academic Publishers,
P.O. Box 17, 3300 AA Dordrecht, The Netherlands.

Sold and distributed in North, Central and South America
by Kluwer Academic Publishers,
101 Philip Drive, Norwell, MA 02061, U.S.A.

In all other countries, sold and distributed
by Kluwer Academic Publishers,
P.O. Box 322, 3300 AH Dordrecht, The Netherlands

Contents

Chapter 8

A GLOBAL PICTURE OF CMES IN THE INNER HELIOSPHERE

N. Gopalswamy
Laboratory for Extraterrestrial Physics, NASA/GSFC, Greenbelt, MD 20771, USA

Abstract This is an overview of Coronal mass ejections (CMEs) in the heliosphere with an observational bias towards remote sensing by coronagraphs. Particular emphasis will be placed on the results from the Solar and Heliospheric Observatory (SOHO) mission which has produced high quality CME data uniform and continuos over the longest stretch ever. After summarizing the morphological, physical, and statistical properties of CMEs, a discussion on the phenomena associated with them is presented. These are the various manifestations of CMEs observed at different wavelengths and the accompanying phenomena such as shocks and solar energetic particles that provide information to build a complete picture of CMEs. Implications of CMEs for the evolution of the global solar magnetic field are presented. CMEs in the heliosphere are then discussed including out-of-the-ecliptic observations from Ulysses and the possibility of a 22-year cycle of cosmic ray modulation by CMEs. After outlining some of the outstanding questions, a summary of the chapter is provided.

1. Introduction

The white-light coronagraph on board NASA's seventh Orbiting Solar Observatory (OSO-7) detected the first "modern" coronal mass ejection (CME) on December 14, 1971 (Tousey, 1973). Just over an year before this detection, Hansen et al. (1971) observed the "rapid decay of the transient coronal condensation" using the Mauna Loa Coronal Activity Monitor during 1970 August 11-12, which is essentially a CME detection. They had also found temporal and spatial association of fast (1000 km s^{-1}) radio sources with the white-light transient feature. In fact, the concept of mass ejections existed as prominence eruptions (ac-

tive and eruptive) since the first scientific observations of Secchi and de la Rue in the late 1800's (see, e.g., Tandberg-Hanssen, 1995): We now know that eruptive prominences form the inner core of many CMEs (see, e. g., House et al., 1981). Mass motions with speeds in the range 500-840 km s^{-1} were inferred from type II radio bursts (Payne-Scott et al., 1947). Moving type IV bursts, indicative of moving magnetized plasma structures in the corona with speeds of several hundred km s^{-1}, were discovered long ago (Boischot, 1957). Slow ($<$ 10 km s^{-1}) and fast (($>$ 100 km s^{-1}) coronal green line transients were also known before the discovery of CMEs (DeMastus et al., 1973). At least two CMEs have been identified in eclipse pictures: during the Spanish eclipse on 1860 July 18 (see Eddy, 1974) and during the Indian eclipse on 1980 February 16 (Rusin et al., 1983). The concept of mass ejection from the Sun was very much in use for explaining geomagnetic storms (Lindemann, 1919). The idea that these plasma ejections might drive shocks (Gold, 1955) was soon confirmed by in situ observations (Sonett, 1964; Gosling, et al., 1968). Interplanetary disturbances were estimated to have a mass of 10^{16} g and an energy of 10^{32} erg (Hundhausen et al., 1970), which we now know are typical of CMEs.

Given the rapid explosion of knowledge on CMEs over the past four decades, it is impossible to review all the published material here. However, complementary reviews include Wagner (1984); Schwenn (1986), Hundhausen (1987), Kahler (1987), Gosling (1997), Howard et al. (1997), Low (1997), Hundhausen (1999), Webb (2002), St. Cyr et al. (2000), Gopalswamy et al. (2003b). In this chapter, we provide an overview of the new developments in CME research, drawing heavily on the results from the Solar and Heliospheric Observatory (SOHO) mission, which has made a significant impact on our current understanding of CMEs. Some of the results to be discussed in this chapter are: (i) Basic statistical properties of CMEs and their solar cycle variation, (ii) special populations such as halo and fast and wide CMEs, (iii) acceleration and deceleration CMEs in the inner heliosphere, (iv) CME-associated eruptive activities, (v) CME-CME interaction, (vi) CMEs in the heliosphere, (vii) role of high-latitude CMEs in solar polar magnetic reversals, (viii) the role of CMEs in modulating the galactic cosmic rays, and (ix) outstanding questions.

2. Solar Source of CMEs

From the early days of CME studies, it is known that CMEs are associated with flares and prominence eruptions (see, e.g. Munro et al., 1979). This means CMEs originate wherever flares and prominences oc-

cur. Flares occur in active regions, which contain high magnetic field with or without sunspots. Active regions consisting of sunspots of opposite polarity seem to produce the most energetic CMEs. Regions on the solar surface where cool prominences are suspended in the corona also contain closed magnetic field structures and they produce spectacular CMEs that carry the prominences out into the interplanetary (IP) medium. Prominences also reside along neutral lines in active regions. Even tiny bipoles observed as bright points in X-rays contain closed field structure producing small jet-like ejections (Shibata et al., 1992), although these are not typically counted as CMEs. CMEs observed at 1 AU by multiple spacecraft have revealed that the "legs of the CME" are probably connected to the Sun, with their feet anchored on either side of the magnetic neutral lines (Burlaga et al., 1981). There was an alternative suggestion that CMEs originated from low-latitude coronal holes (Hewish et al., 1985), but now it is fully established that CMEs originate from closed magnetic field regions on the Sun (see, e.g. Harrison, 1990). However, filaments near coronal holes seem to have a proclivity for eruption (Webb et al., 1978; Bhatnagar, 1996), which suggests that such eruptions can be mistakenly associated with coronal holes. Closed magnetic structure, thus, seems to be the basic characteristic of CME-producing regions on the Sun, which means the energy needed to carry billions of tons of ionized plasma in to the heliosphere must ultimately come from the magnetic field itself. How this energy is stored in the coronal magnetic fields and what triggers the energy release are topics of current research and debate.

3. CME Morphology

The general appearance of a CME is shown in Fig. 1. The earliest activity observed on the Sun was a prominence eruption observed in microwaves from the southeast quadrant of the Sun. The prominence eruption was also observed by the Extreme-ultraviolet imaging telescope (EIT,) on board SOHO. In running difference images, a faint depletion can be seen surrounding the prominence. There are two dimming regions (D), one on each side of the neutral line, that mark the pre-eruption location of the prominence. After the eruption, a post eruption arcade forms (denoted by AF) with its individual loops roughly perpendicular to the neutral line. The dimming regions are located just outside the arcade, but at the opposite ends of the arcade axis. "Coronal dimming" represents the reduction in brightness in a certain region of the corona as compared to an earlier period, typically on either side of the polarity inversion line underlying the CME (see Sterling, 2003 for a review).

Dimming is a change in the physical conditions (density and temperature) of the emitting plasma, typically observed in X-rays (Hudson, 1999), EUV (Gopalswamy and Thompson 2000) and occasionally in microwaves (Gopalswamy, 2003b).

The white-light CME first appears an hour later above the occulting disk of the Large Angle and Spectrometric Coronagraph (LASCO) in the same position angle as the eruptive prominence. The bright frontal structure is loop-shaped, inside of which there is a bright core. From the morphological, position angle, and temporal coincidences, it is clear that the core seen in white light is nothing but the prominence. The EUV and microwave data alone give a speed of $\sim$ 97 km s^{-1} that became higher by the time the CME entered the LASCO field of view. The legs of the frontal structure are thought to extend below the occulting disk with the feet located on either side of AF. There is a conspicuous void that separates the prominence core and the frontal structure, commonly referred to as cavity containing less coronal material and strong magnetic field. The cavity is also thought to have a flux-rope magnetic structure with the legs of the rope anchored on either side of the neutral line. The core and the frontal structure was about 5 R$_\odot$ by the time the CME left LASCO FOV. The average speed of the CME was 770 km s^{-1}. This CME could be thought of as a typical three-part structure CME. The classical three-part structure (Hundhausen et al., 1988) is well observed only in CMEs that are associated with prominences erupting from quiet regions. When prominences erupt from active regions, it is often difficult to discern the three-part structure. Prominences in active regions are thin and low-lying and may be heated and ionized before arriving in the coronagraph field of view.

Figure 2 shows another CME, in which the three-part structure is not very clear. This CME originated from an active region slightly behind the southwest limb. The white light CME was highly structured, but not similar to the one in Fig. 1. The CME was very dense with a compact internal structure that moved behind the frontal structure. The frontal structure was also flat-topped. The front moved with speed of $\sim$ 2500 km s^{-1}, while the inner core had a speed of 1500 km s^{-1}. The core was much smaller within the overall volume of the CME. The main body of the CME is seen distinct from the two streamer displacements on either side of the CME. These disturbances are also likely to be present away from the plane of the sky.

From the above examples one can infer that a white-light CME is highly structured and is three-dimensional. Stereoscopic observation of a few CMEs by the Helios photometer and the Solwind coronagraph essentially demonstrated the 3D nature of CMEs (Jackson, 1985), and

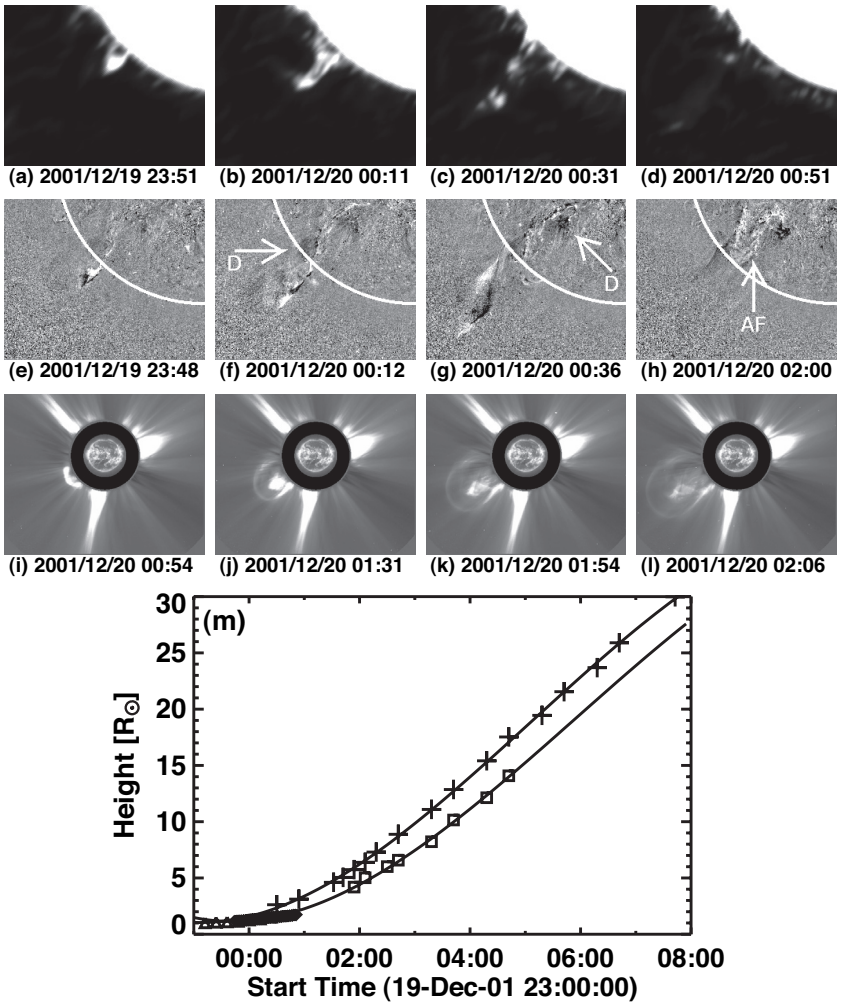

Figure 8.1. Morphology of a three-part CME and the associated solar surface activities: (a-d) prominence eruption in microwaves, (e-h) SOHO/EIT difference images showing the prominence eruption in EUV with dimming (D) and arcade formation (AF), (i-l): SOHO/LASCO images showing the core, void and frontal structure of the CME, and (m) height-time plots of the frontal structure ('plus' symbols, white-light) and the prominence from various sources (EUV -triangles; microwave - diamonds and white light -squares).

this was confirmed by numerical simulations (e. g., Crifo et al., 1983). LASCO has observed a number of different morphological types, which are yet to be surveyed and classified. Some CMEs are interpreted as flux ropes (Chen et al., 2000; Plunkett et al., 2000). Some CMEs have

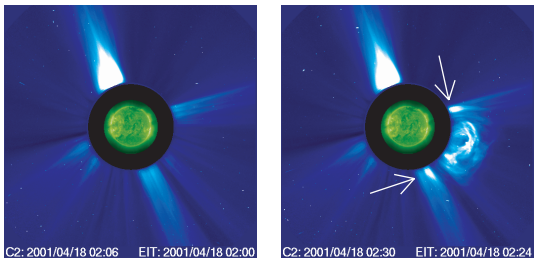

Figure 8.2 LASCO images of (left) the pre-event corona and (right) the 2001 April 18 CME. The pre-event corona can be seen on the left. Arrows point to the compressed regions of the streamers on either side of the CME.

voids with no prominence in them (Gopalswamy et al., 2001d). Jets and narrow CMEs with no resemblance to the three-part structure have also been observed (Wang and Sheeley, 2002; Yashiro et al., 2003).

4. Physical Properties

Since the material in CMEs is already present in the corona before ejection, we expect the CME to be at the coronal temperature. However, the core of the CME is prominence material and hence can be quite cool (4000 - 8,000 K). Not much is known about cavity, but is also thought to be at coronal temperatures. White light coronagraphs detect just the mass irrespective of the temperature. Non-coronagraphic observations are needed to infer temperatures. The magnetic field of the CMEs near the Sun is also unknown. Radio observations indicate a magnetic field strength of $\leq$1 G in the corona at a heliocentric distance of 1.5 $R_\odot$ (see, e.g., Dulk and McLean, 1978). Gyroresonance emission from active regions indicate that coronal magnetic fields above sunspots can be as high as 1800 G (White et al., 1991). When an eruption occurs in a strong field region, one might expect a strong field in the resulting CME. The field strength in the prominences are better known (Tandberg-Hanssen, 1995): 3-30 G in quiescent prominences and 20-70 G in active prominences, occasionally exceeding 100 G (Kim and Alexeyeva, 1994). The magnetic field in the cavity is virtually unknown. The idea that the cavity is a magnetic flux rope may have some support from the numerous dark threads observed in high resolution eclipse images (Engvold, 1997). The density in the inner corona is typically 10^{8-9} cm^{-3} and is expected to be present in the frontal structure of CMEs close to the Sun. Density estimates from white light observations (see e.g., Vourlidas et al., 2002) radio (Gopalswamy et al., 1993) and ultraviolet observations (Ciaravella et al., 2003) are consistent with such densities. The prominences are much denser (10^{10-11} cm^{-3}). The cavity is certainly of lower density compared to the frontal structure and prominence core.

Table 8.1. Summary of Space borne coronagraph observations of CMEs from OSO-7 (Tousey, 1973), Skylab (MacQueen et al., 1974), Solwind (Michels et al., 1980), SMM (MacQueen et al., 1980), and SOHO (Brueckner et al., 1995).

Coronagraph	OSO-7	Skylab	Solwind	SMM	LASCO
Epoch	1971	1973-74	1979-85	1980,84-89	1996-2003
FOV ($R_\odot$)	2.5-10	1.5 - 6	3 - 10	1.6 -6	1.2-32
# CMEs recorded	27	115	1607	1206	8008
Mean Speed (km/s)	-	470	460	350	489
Mean Width (deg.)	-	42	43	47	47
Mass (10^{15} g)	-	6.2	4.1	3.3	1.6

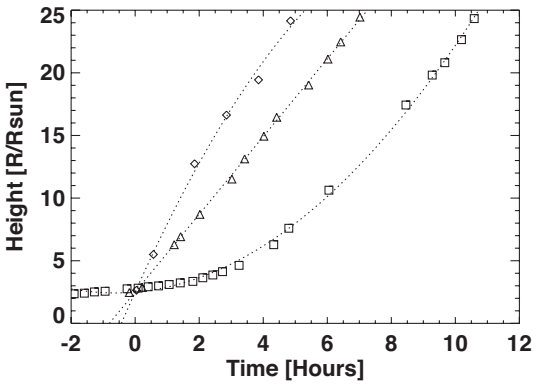

Figure 8.3 Height-time measurements of three representative CMEs observed by SOHO/LASCO: the accelerating CME of June 21, 1998 (squares), the constant speed CME of February 17, 2000 (triangles), and the decelerating CME of May 11, 1998 (diamonds). The curves are best-fit polynomials (linear for the constant speed case and quadratic for the other two). The plots are normalized to the time the CMEs reach 2.5 $R_\odot$. (See Gopalswamy et al., 2001e for more details).

5. Statistical Properties

The OSO-7 coronagraph detected only 27 CMEs over a period of 19.5 months. The Skylab ATM coronagraph recorded 110 CMEs during its 227 days of operation. The number shot up by an order of magnitude when the Solwind coronagraph on board P78-1 and the Coronagraph/Polarimeter on board the Solar Maximum Mission (SMM/CP) became operational. SOHO/LASCO has detected more than 8000 over a period of 8 years (1996-2003), confirming that CMEs are a common phenomenon. Table 1 summarizes these observations and updates a previous compilation by Hundhausen (1997).

5.1 CME Speed

Mass motion is the basic characteristic of CMEs, quantified by the speed. Coronagraphs obtain images with a certain time cadence, so when a CME occurs, the leading edge progressively appears at a greater heliocentric distance. By tracking a CME feature in successive frames, one can derive the speed of the feature. It must be pointed out that the height-time measurements are made in the sky plane so all the derived parameters such as speed are lower limits to the actual values. Figure 3 shows three examples of height-time (h-t) plots. A straight-line fit to the h-t measurements gives the average speed within the coronagraph field of view, but it may not be suitable for all CMEs. For studying the variation of speed, one has to use higher order fits. For SOHO/LASCO CMEs, the sky plane speed from linear fit ranges from tens of km s^{-1} to >2500 km s^{-1}, with an average value of 489 km s^{-1} (see Table 1 and Fig. 4). Skylab and P78-1 CMEs had similar average speeds, but the SMM value was relatively low (Hundhausen, 1997). The discrepancy may be due to poor data coverage and the inability to measure the speeds of many of the observed CMEs (Gopalswamy et al., 2003b). For similar reasons, the SMM data did not show a significant difference in the average speed of CMEs between solar activity minimum and maximum (Hundhausen, 1999), although other measurements did indicate a definite increase (Howard et al., 1985). SOHO data confirmed the increase beyond any doubt (Gopalswamy et al., 2003b) as demonstrated in Figure 5.

SOHO detected a number of CMEs with speeds exceeding 2000 km s^{-1} (Gopalswamy et al., 2003c). The largest speed (2657 km s^{-1}) observed was for the 2003 November 04 CME during the largest flare of cycle 23. These ultrafast CMEs constitute only a tiny fraction (25/8008) of the total number of CMEs, which suggests a possible upper limit to the energy that goes into mass motion in CMEs.

5.2 CME Acceleration

All CMEs have positive acceleration in the beginning as they lift off from rest (the propelling force (F_p) exceeds gravity (F_g) and other restraining forces). The moment a CME lifts off, it is subject to an additional retarding force - the drag, given by $F_d = CA\rho$—V_{cme}-V_{sw}—(V_{cme}-V_{sw}), where C is the drag coefficient (Chen, 1989; Cargill et al., 1996), A is the surface area of the CME, ρ is the plasma density, V_{cme} is the CME speed and V_{sw} is the solar wind speed (negligible close to the Sun). The three types of h-t profiles shown in Fig. 3 reflect various combinations of propelling and retarding forces: the accelerating profile

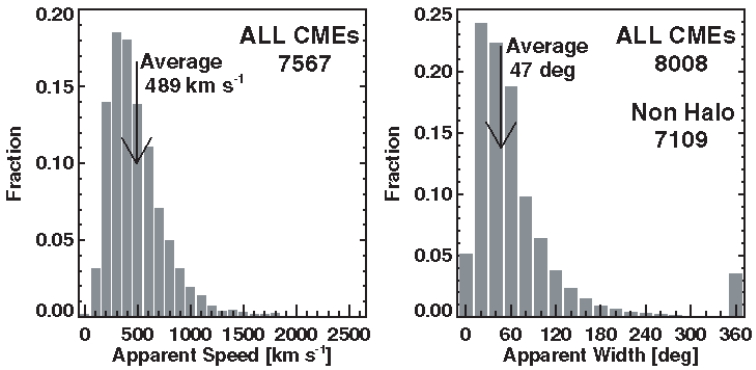

Figure 8.4. The speed (left) and width (right) distributions of all CMEs from 1996 to 2003. The width of a CME is measured as the angle subtended by the outer edges of the CME at the Sun center. The speed is obtained by straight-line fit to the height-time measurements. Even though 8008 CMEs were detected, the speed could be measured only for 7567 CMEs, giving an average speed of 489 km s^{-1}. The average width of 47° corresponds to the 7109 non-halo (width ≤120°) CMEs. Inclusion of all CMEs yields a width of 67°. The last bin in the width distribution contains the full halo CMEs, which constitute only ∼3.5% of all CMEs. The fraction of CMEs with width ≥120° is ∼11%. The speed and width are sky-plane projections and no attempt was made to correct for projection effects.

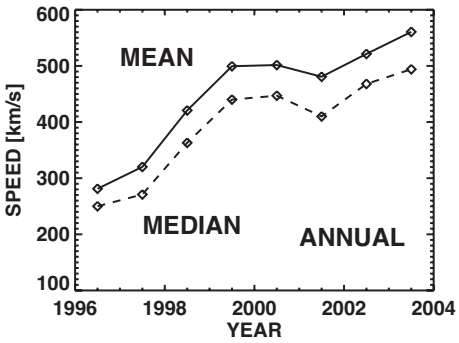

Figure 8.5 Annual mean and median speeds of SOHO/LASCO CMEs from 1996 to 2003 showing the clear increase towards solar activity maximum. Higher speeds prevailed even after the solar activity maximum.

indicates that the propelling force is still active in pushing the CME outward. The constant-speed and decelerating profiles suggest that the retarding forces either balance or exceed the propelling force. The average acceleration obtained from MLSO K-coronameter (FOV = 1.2 - 2.7 $R_\odot$) data is generally positive and high compared to those obtained from SMM (FOV = 1.8 - 5 $R_\odot$) and LASCO (FOV = 2 - 32 $R_\odot$) coronagraphs (Burkepile et al., 2002). Furthermore, combining data below the occulting disk with those from above clearly indicate that the ac-

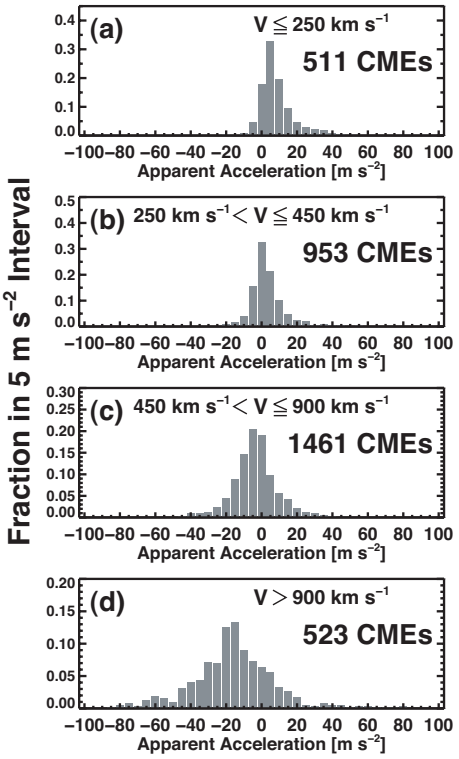

Figure 8.6 The average acceleration of CMEs (1996-2003) within the LASCO FOV for various speed ranges. Note the tendency for deceleration for faster CMEs.

celeration is variable (St. Cyr et al., 1999; Gopalswamy and Thompson, 2000; Wood et al., 1999; Zhang et al., 2001). Measurements of individual events give accelerations generally below a few km s^{-2}. Gopalswamy et al. (2001b) found that fast ($V > 900$ km s^{-1}) CMEs predominantly decelerated within LASCO FOV, suggesting that the deceleration is very general and must be due to drag. A number of recent studies suggest that the propelling forces fade out at heights below ~ 4 $R_\odot$ (Chen and Krall, 2003), so drag must play a significant role within LASCO FOV. Statistical analyses of the observed acceleration support this interpretation (Yashiro et al., 2004). Figure 6 shows the distribution of CME accelerations (a) for various speed ranges: (i) slow CMEs ($V_{cme} \leq 250$ km s^{-1}) are accelerated (median $a = 6$ m^{-2}), (ii) CMEs with speeds in the vicinity of solar wind speed (250 km $s^{-1} < V_{cme} \leq 450$ km s^{-1}) show little acceleration (median $a = 1.6$ m^{-2}), (iii) CMEs with speeds above the solar wind speed (450 km $s^{-1} < V_{cme} \leq 900$ km s^{-1}) show predominant deceleration (median a = -4 m^{-2}), and the fast CMEs (V > 900 km s^{-1}) show clear deceleration (a = -16 m^{-2}). This behavior is also found when CME propagation is considered over the inner heliosphere (Gopalswamy et al., 2000a; Lyndsay et al., 1999).

5.3 CME Width

CME angular span (also referred to as CME width) is measured as the position angle extent in the sky plane. For CMEs originating from close to the limb, the measured width is likely to be the true width. For CMEs away from the limb, the measured width is likely to be an overestimate. Many CMEs show increase in width as they move out, so measurements are made when the width appears to approach a constant value. The average of the width distribution of SOHO/LASCO CMEs shown in Fig. 4 is 47° when we exclude CMEs with width > 120° (because they are unlikely to be actual widths). Annual averages of non-halo CME widths range from 47° to 61° (Yashiro et al., 2004); the average width is the smallest during solar minimum, peaks just before the maximum and then declines through the maximum. The average widths obtained from Skylab (42°), SMM (47°) and Solwind (43°) are remarkably similar and in good agreement with LASCO results (see Table 1). This is true only when we exclude CMEs with widths exceeding 120°, a population not present in significant numbers in pre-SOHO data. The average width is 67° when we include all CMEs (similarly to St. Cyr et al., 2000, who found a value of 72° during the rise phase of cycle 23).

5.4 CME Latitude

The latitude distribution of CMEs depends on how closed field regions are distributed on the solar surface. CME latitude is obtained from the central position angle of the CME, assuming that CMEs propagate radially away from the solar source region (Howard et al., 1986; Hundhausen 1993; Gopalswamy et al., 2003a). This assumption may not be always valid especially during the solar minimum periods when the CME trajectory is likely to be controlled by the global dipolar field of the Sun (Gopalswamy et al., 2000c). Figure 7 shows a plot of the CME latitude as a function of time along with the maximum excursions of the heliospheric current sheet (a good indicator of the presence of closed field structures at high latitudes) for CMEs associated with prominence eruptions. During the rising phase of cycle 23 (1997-1998), the CME latitudes were generally close to the equator and subsequently spread to all latitudes. During the maximum phase, there are many polar CMEs and the number of such CMEs was larger in the southern hemisphere and occurred over a longer time period than in the north. This behavior of CME latitudes with the solar activity cycle is consistent with previous measurements from Skylab/ATM (Hildner, 1977; Munro et al., 1979), P78-1/Solwind (Howard et al., 1985; 1986) and SMM/CP (Hundhausen, 1993).

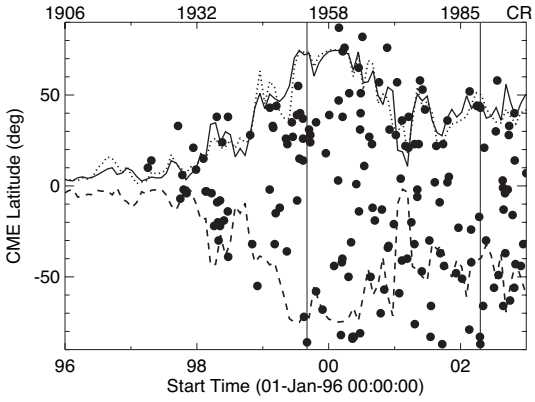

Figure 8.7 Latitudes of CMEs (filled circles) with known solar sources (identified from microwave prominence eruptions), plotted as a function of time. The Carrington Rotation numbers are marked at the top (CR). The dotted and dashed curves represent the tilt angle of the heliospheric current sheet in the northern and southern hemispheres, respectively; the solid curve is the average of the two. The two vertical lines indicate the start and end of the high-latitude CME activities.

5.5 CME Occurrence Rate

A CME rate of 0.5 CMEs/day was derived from the OSO-7 coronagraph data (Tousey et al., 1974). Skylab data indicated an average rate of ~ 1/day with a good correlation between sunspot number (SSN) and CME rate (Hildner et al., 1976). Combining Skylab, SMM, Helios (Photometer), and Solwind observations, Webb and Howard (1994) found a rate of 0.31 to 0.77 CMEs/day for the solar minimum years and 1.75 to 3.11 CMEs/day for the solar maximum years. The correlation between CME rate and SSN was also found to hold when the data were averaged over Carrington Rotation periods (Cliver et al., 1994). The early indication from SOHO was that the solar-minimum rate (0.8/day) was much higher than the uncorrected rate during previous minima (Howard et al., 1997); when more data came in, St. Cyr et al. (2000) concluded that the rate corresponding to the rise phase of cycle 23 was not significantly different from pre-SOHO observations. It finally turned out that the SOHO CME rate averaged over Carrington Rotation periods increased from less than 1 during solar minimum (1996) to slightly more than 6 during maximum (2002) (see Fig. 8). The solar-maximum rate of SOHO CMEs was nearly twice the highest corrected rate (3.11 per day) reported for previous cycles (Webb and Howard, 1994). We attribute this primarily to the better sensitivity and the enormous dynamic range (16000:1) of the LASCO coronagraphs. Additional factors include larger field of view and more uniform coverage over long periods of time (Howard et

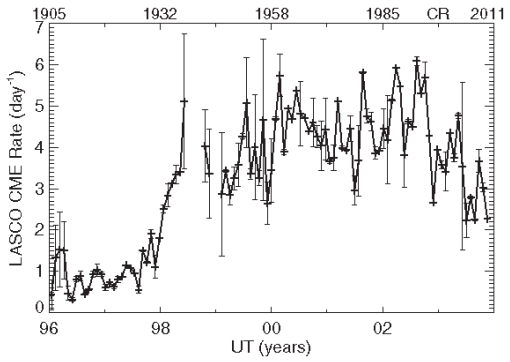

Figure 8.8 The CME occurrence rate (day^{-1}) averaged over Carrington Rotation (CR) periods as a function of time for the interval 1996-2003. There was a large data gap due to SOHO mission interruption during June to October 1998 and a smaller gap during January-February, 1999. The CR numbers are marked at the top. The error bars are based on the amount of SOHO downtime during each CR.

al., 1997). Note that LASCO CME rate is not corrected for duty-cycle, but an analysis by St. Cyr et al. (2000) suggested that such a correction may not be necessary for the LASCO data.

While SOHO data also confirmed the high correlation (r=0.86) between SSN and CME rate, the slope of the regression line was significantly different from pre-SOHO values (see Cliver et al., 1994) because of the higher maximum rate (Gopalswamy et al., 2003b). Furthermore, the CME rate peaked in CR 1993 (August 13-September 9, 2002), well after the maximum of the sunspot cycle (CR 1965, July 10-August 6, 2000). Figure 9 compares the CME rate with SSN averaged over longer periods of time (13 CRs). Clearly both have double peaks, but they are shifted with respect to each other. The difference between the two rates seems to be due the fact that CMEs originate not only from the Sunspot regions, but also from non-sunspot (quiescent filament) regions.

5.6 CME Mass and Energy

Skylab data indicated that a single CME could account for a mass of $\sim 4\times10^{15}$ g (Gosling et al 1974), which was soon confirmed (Hildner, 1977; Poland et al, 1981; Jackson and Howard, 1993; Howard et al, 1984). The mass in a CME is estimated by determining the CME volume and the number of electrons in the CME with the assumption that the CME is a fully ionized hydrogen plasma with 10% helium. Mass estimates have also been made using radio (Gopalswamy and Kundu 1992; 1993; Ramesh et al., 2003) and X-ray observations (Rust and Hildner, 1976; Hudson et al., 1996; Gopalswamy et al., 1996; 1997a; Hudson and Webb,

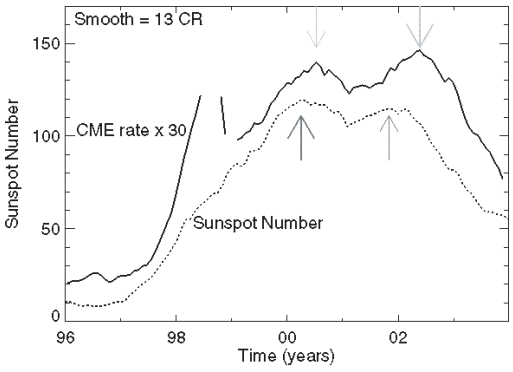

Figure 8.9 Time evolution of Sunspot number (SSN) and CME occurrence rate averaged over 13 Carrington Rotation periods. No smoothing was done for CME rates during the interval 1998 June to 1999 February, when there were large data gaps. The CME rate was multiplied by a factor of 30 to fit the scale. The arrows point to the two largest peaks in SSN and CME rate.

1997; Sterling and Hudson 1997; Gopalswamy and Hanaoka 1998). The radio and X-ray estimates (10^{14} - 10^{15} g) are generally lower than, but well within the range of, the white-light mass values. It must be pointed out that the X-ray and radio mass estimates of CMEs correspond to regions close to the Sun whereas the white light estimates correspond to larger heights (a few $R_\odot$). The X-ray and radio techniques are based on the thermal emission properties of the CME plasma (as opposed to Thomson scattering in white light), and hence provide an independent cross-check for mass estimates. However, routine estimates are done only in white light. Figure 10 shows a summary of mass and energy properties of 4297 LASCO CMEs for the period 1996-2002 (see also Table 1). The average mass (1.6×10^{15} g) of LASCO CMEs is somewhat lower than those of Solwind and SMM/CP CMEs (Vourlidas et al., 2002). This may be due to the fact that LASCO was able to measure CMEs of mass as low as 10^{13} g: $\sim$15% of CMEs had masses less than 10^{14} g. From the energy distribution shown in Fig. 10, it is found that the average (median) kinetic energy of the 4297 CMEs is 2.4×10^{30} erg (5×10^{30} erg), while the average (median) potential energy is 2.5×10^{30} erg (9.6×10^{30} erg). Figure 10 also shows the mass density (amount of mass in grams that corresponds to each pixel of the CME in LASCO images) as a function of height. The mass density increases rapidly to about 8 $R_\odot$ and then levels off. The fractional number of CMEs in each height bin (shown by the dashed-line histogram in the lower left panel of Fig. 10), suggests that those CMEs that reach greater heights have the largest mass density. We can see that $\sim$20% of CMEs reach their maximum mass at a height of $\sim$5 $R_\odot$, while almost half of the CMEs reach it within the LASCO/C2 FOV. In an earlier study, increases in mass by

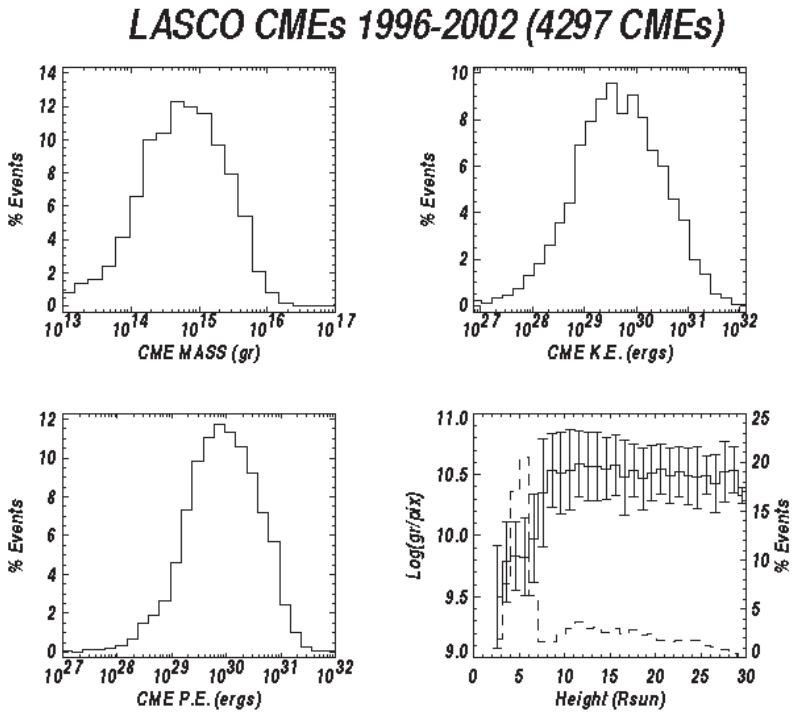

Figure 8.10. CME mass and energy (kinetic - K.E., and potential - P. E.) distributions and the evolution of mass density (grams/pixel) as a function of heliocentric distance. In the bottom right panel, the histogram (dashed line) shows that most of the CMEs were detected within the height range of increasing mass density. Not all detected CMEs have been included because mass measurements require (i) a good background image, (ii) three consecutive frames with CMEs, and (iii) CMEs well separated from preceding CMEs. Courtesy: A. Vourlidas.

a factor of up to 3 were found from the corona to the interplanetary medium (Jackson and Howard, 1993). Large mass increases (by a factor of 5-10) were also found from Yohokoh/SXT (Gopalswamy et al., 1996, 1997a) and SOHO/LASCO (Howard et al., 1997) observations. It is important to point out that LASCO movies show continued outflow of mass in the aftermath of CMEs for a day or so. A systematic study is needed to identify the origin and the magnitude of this mass compared to the CME mass obtained from snapshot images.

5.7 Halo CMEs

Halo CMEs are so named because of their appearance as approximately circular brightness enhancements surrounding the occulting disk.

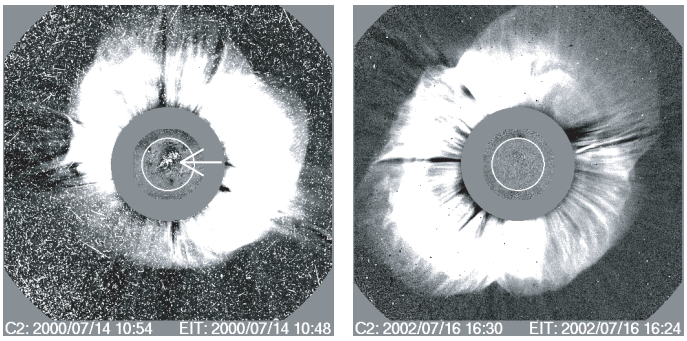

Figure 8.11. Front-side (left) and backside (right) full halo CMEs from SOHO/LASCO. The arrow points to the EUV eruption seen in the SOHO/EIT difference image superposed on the LASCO difference image; no EUV activity was observed for the backside halo because the solar source was occulted.

Although halo CMEs are known from pre-SOHO observations (Howard et al., 1982), their prevalence became clear in the SOHO data (Webb et al., 2000; St. Cyr et al., 2000; Webb, 2002; Gopalswamy et al., 2003b; Michalek et al., 2003; Yashiro et al., 2004). CMEs heading towards and away from the observer can appear as halos. Figure 11 shows two halo CMEs, one originating from the visible disk of the Sun and the other from the backside. From coronagraph images alone it is impossible to tell which way the halos are heading, so we need coronal images (such as the SOHO/EIT difference images in Fig. 11) to check if there is disk activity. It must be noted that the circular appearance of halos is due to projection on the sky plane. Figure 12 shows two CMEs originating from the same active region (AR 10486) when it was close to the disk center on 2003 October 28 and near the west limb on 2003 November 4. To an observer located above the west limb the October 28 event would appear as an east limb event, while the November 4 event would appear as a halo. Coronagraphs on the two STEREO spacecraft should be able to provide such a multiview for single CMEs. CMEs originating from close to the limb appear as asymmetric or partial halos (Gopalswamy et al. 2003b). Limb CMEs sometimes appear as halos because of faint enhancements seen above the opposite limb. These extensions may be shocks or magnetosonic waves propagating perpendicular to the direction of ejection (Sheeley et al., 2000).

The annual totals of halo CMEs are compared with those of the general population in Fig. 13. The number of halo CMEs had a broad peak during the solar maximum phase (2000-2002). However, the fraction of halo CMEs is always less than 5% (see also Fig. 4). The largest fraction resulted in 1997, during the rising phase of solar cycle 23. For the solar

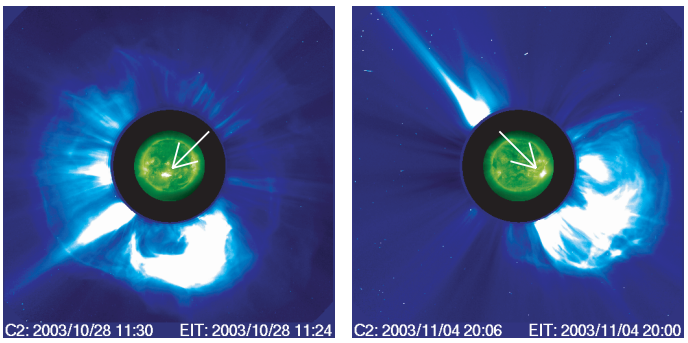

Figure 8.12. Two CMEs from the same active region (AR 10486) and similar speeds: (left) halo CME on 2003 October 28 (2459 km s^{-1}), and (right) limb CME on 2003 November 4 (2657 km s^{-1}). The arrows point to the EUV brightenings in the active region as observed by SOHO/EIT.

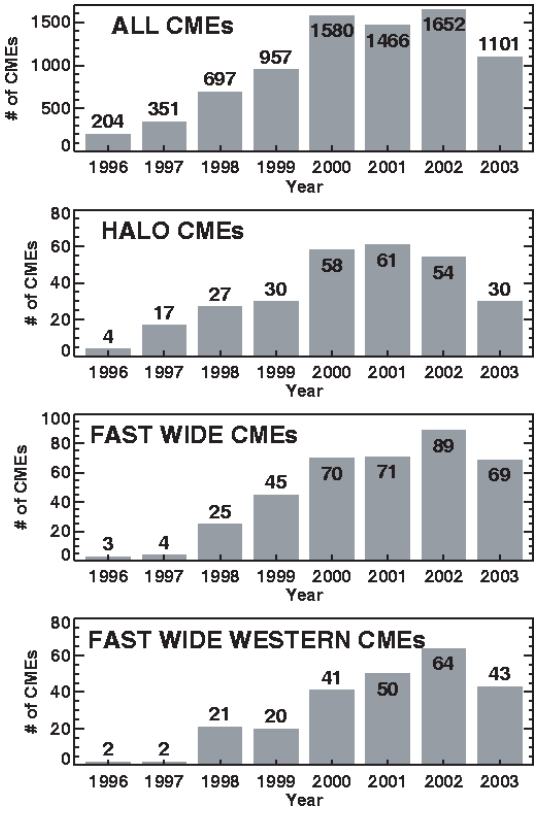

Figure 8.13 Annual numbers of the general population of CMEs compared with those of the special populations: halo, fast and wide, and fast-and-wide western CMEs. Fast and wide CMEs have speed > 900 km s^{-1} and width $> 60°$. Fast and wide western CMEs are the same as fast and wide CMEs, but their span includes position angle 270°. The numbers in each bin are marked. The special populations are similar in number but constitute a small fraction of the general population.

maximum phase (years 2000-2002), the number of halo CMEs exceeded 50 per year (100 per year if CMEs with width $> 180°$ are considered).

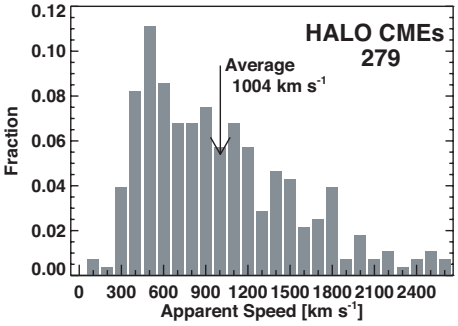

Figure 8.14 Speed distribution of the 279 halo CMEs for the period 1996-2003. Note that there are very few halo CMEs with speeds less than 300 km s^{-1} (most of these are from the solar minimum period).

What is special about halo CMEs? In principle, even narrow CMEs originating on the disk or backside should eventually become halo CMEs. These CMEs have to move far enough for their flanks to be "visible". Because of their large angle with respect to the sky plane and the distance from the Sun, they may not be detected by coronagraphs. Studying all the halo CMEs detected by LASCO, Yashiro et al. (2004) found that the average speed of the halo CMEs is roughly twice that of the general population of CMEs. Figure 14 shows the speed distribution of the 279 halo CMEs from 1996 to 2003. The average speed of the halo CME population shown is 1004 km s^{-1}, compared to 489 km s^{-1} for the general population (see Fig. 4). Thus, most of the halo CMEs seem to belong to a population known as fast-and-wide CMEs (speed (> 900 km s^{-1} and width $> 60°$), which are known for driving shocks and producing solar energetic particles and long-wavelength radio emission (Gopalswamy et al., 2003c). While it is not uncommon for CMEs from the eastern hemisphere to be associated with SEP events at Earth, western hemispheric fast and wide CMEs result in prompt increase of SEP intensity at 1 AU.

6. Associated Activities

CMEs are associated with a number of phenomena starting all the way from the chromosphere (H-alpha flare ribbons, Moreton waves), and the corona (dimming, arcade formation, X-ray flares, prominence eruptions, X-ray and EUV ejecta, EUV wave transients, metric radio bursts) to the heliosphere (magnetic clouds, interplanetary radio bursts, shocks and energetic particles), that are observed as mass motion, waves and electromagnetic radiation. H-alpha and soft X-ray flares, prominence eruptions, and soft X-ray and EUV ejecta provide vivid pictures of the eruption during its early stages, generally not accessible to coronagraphs. Radio bursts produced by shocks (type II) and moving magnetic structures (type IV), are closely related to CMEs. Phenomena such as CME-related dimming (Hudson, 1999; Gopalswamy, 1999; Gopalswamy and Thomp-

son, 2000; Klassen et al., 2000), EUV wave transients (Thompson et al., 1999; Gopalswamy and Thompson, 2000; Mann et al., 1999; Biesecker et al., 2002), and arcade formation (Hanaoka, 1994; Gopalswamy et al., 1999) have become benchmark signatures that are commonly used in identifying the solar sources of CMEs, in addition to the traditional H-alpha flare locations. SOHO's Ultraviolet Coronagraph Spectrometer (UVCS, Kohl et al., 1995) has turned out to be a useful source to estimate the true speed of CMEs (as opposed to sky plane speeds) and a number of physical parameters such as density and temperature (see, e.g., Ciaravella et al., 2003).

6.1 Flares and CMEs

Early statistical studies (see, e.g., Munro et al., 1979; Kahler, 1992) showed that $\sim$ 40% of CMEs were associated with H-alpha flares and almost all flares (90%) with H-alpha ejecta were associated with CMEs. Thus the "mass motion" aspect of flares seems to be critical for a flare to be associated with CME. Flares have been classified (see, e.g. Pallavicini et al., 1977; Moore et al., 1999) as impulsive (short-duration ($<$ 1h), compact (10^{26}-10^{27} cm^3), and low-lying (10^4 km)) and gradual (long duration (hours), large volumes (10^{28}-10^{29} cm^3), and great heights (10^5 km)). The probability of CME-flare association increases with flare duration (Sheeley et al., 1983): 26% for duration $<$ 1h and 100% for duration $>$ 6 h. It must be pointed out that some major flares associated with large-scale CMEs are not long-duration events (Nitta and Hudson, 2001; Chertok et al., 2004). Currently, there are three ideas about the flare-CME relationship: 1. Flares produce CMEs (see, e.g., Dryer, 1996), 2. Flares are byproducts of CMEs (Hundhausen, 1999), and 3. Flares and CMEs are part of the same magnetic eruption process (Harrison 1995; Zhang et al., 2001). Studies on temporal correspondence between CMEs and flares have concluded that CME onset typically precedes the associated X-ray flare onset by several minutes (e.g. Harrison 1991). This observational fact is considered to be a serious difficulty for flares to produce CMEs (Hundhausen, 1999). The flare process - reconnection that forms post flare loops - can be thought of as the force that propels overlying loops as CMEs (Anzer and Pnueman, 1982). Kahler et al. (1989) argued against such a model because they could not find evidence for a flare impulsive phase affecting the height-time history of CMEs. Zhang et al. (2001) investigated four CMEs and compared their time evolution with GOES X-ray flares. They found that the CMEs started accelerating impulsively until the peak of the soft X-ray flare, consistent with an earlier result that flare-associated CMEs are in gen-

eral faster than other CMEs (MacQueen and Fisher, 1983). There is also weak correlation (r = 0.53) between soft X-ray flare intensities and associated CME energies (Hundhausen, 1999; Moon et al., 2002). The fact that flares with H-alpha ejecta are closely related to CMEs suggests that we need to understand how the free energy in the eruptive region is partitioned between heating (soft X-ray flares) and mass motion (CMEs). The connection between flares and CMEs needs to be revisited especially because of the availability of high quality multiwavelength data on flares and CMEs.

6.2 Prominence Eruptions

Prominence eruptions (PEs) are the near-surface activity most frequently associated with CMEs (Webb et al., 1976; Munro et al., 1979; Webb and Hundhausen, 1987; St. Cyr and Webb, 1991): 70% of CMEs are associated with PEs (Munro et al. 1979). Reverse studies indicate that the majority of PEs are associated with CMEs (Hori and Culhane, 2002; Gopalswamy et al., 2003a). Using microwave PEs, Gopalswamy et al. (2003a) found that (i) 73% of PEs had CMEs, while 16% had no CMEs at all, and the remaining PEs were associated streamer changes; (ii) the PE trajectories could be broadly classified as radial (R) and Transverse (T); (iii) most of the R events were associated with CMEs and the eruptive prominences attained larger heights, while most of the T events were not associated with CMEs; (iv) almost all of the PEs without CMEs were found to be T events (in which material does not leave the Sun). These results are consistent with those of Munro et al. (1979) who found that virtually all prominences that attained a height of at least 1.2 $R_\odot$ were associated with *Skylab* CMEs. The source locations of CMEs and prominences spread to all latitudes towards the solar maximum in a similar fashion. During solar minimum, the central position angles of CMEs tend to cluster around the equator, while those of PEs were confined to the latitudes of active region belt, reflecting the stronger influence of the solar dipolar field on CMEs during solar minimum.

What is the physical connection between prominences and CMEs? Case studies have shown that eruptive prominences can be traced into the inner parts of the bright core (House et al. 1981; Illing and Athay, 1986; Gopalswamy et al., 1998), and this has been confirmed by statistical studies. There is also a close correspondence between the projected onset times of CMEs and PEs (Gopalswamy et al., 2003a). These results indicate that PEs form an integral part of CMEs. However, PEs are considered as a secondary phenomenon to the CME process because PEs

may not have enough energy to drive CMEs (Hundhausen, 1999). Filippov (1998) has a different result: CMEs can be caused by the eruption of inverse-polarity prominences. Runaway reconnection in the magnetic field of the prominence is also thought to be fundamental for the onset of CMEs (Moore et al., 2001).

6.3 Are There Two types of CMEs?

On the basis of speed-height profiles of a dozen CMEs observed by the MLSO K-coronameter, MacQueen and Fisher (1983) suggested that different acceleration mechanisms may be operating in CMEs associated with prominence eruptions and flares. The flare-related CMEs were faster and characterized by constant speed, while the prominence-related CMEs were slower and accelerating within the coronameter FOV (see also St. Cyr et al., 1999). Tappin and Simnett (1997) used 149 LASCO CMEs and found that the constant speed CMEs were generally faster. Examples of constant speed and accelerating h-t profiles were also reported by others (Sheeley et al., 1999; Andrews and Howard, 2001; Gopalswamy et al., 2001b). The travel time of flare-related solar disturbances has also been found to be generally shorter than that of prominence-related ones (Park et al., 2002). Studying a much larger sample of LASCO CMEs, Moon et al. (2002) found a clear difference in speeds of flare-related (759 km s^{-1}) and prominence-related (513 km s^{-1}) CMEs. The flare-related CMEs also showed a tendency for deceleration, but this probably reflects the fact that they are faster (see Gopalswamy et al., 2001b). The question is whether the speed difference is qualitative or quantitative given that CMEs of both types involve closed magnetic regions with filaments. Studying the acceleration of CMEs, Chen and Krall (2003) conclude that one mechanism is sufficient to explain flare-related and prominence-related CMEs.

6.4 X-ray Ejecta

Klimchuk et al. (1994) found that the properties of 29 X-ray eruptions from Yohkoh/SXT were similar to those of white-light CMEs. Although they did not compare their data with white light observations, it is likely that they correspond to the frontal structure. X-ray ejecta were also frequently seen by SXT (see, e.g., Shibata et al., 1995), but their white-light counterpart was not checked. Gopalswamy et al. (1997b) reported an X-ray eruption followed by a disconnected X-ray plasmoid. Checking white-light data from MLSO, they concluded that the eruption was associated with a CME. The plasmoid was also associated with a moving type IV burst, which suggested that the X-ray plasmoid must have

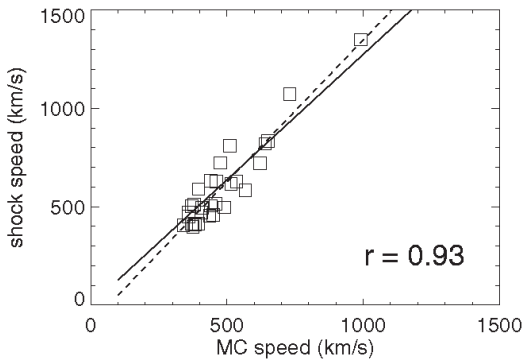

Figure 8.15 Scatter plot of shock speed versus magnetic cloud (MC) speed for a number of events detected by Wind at 1 AU. The correlation coefficient (r) is 0.93. The solid line is the best-fit to the data points. The dashed line is the gas dynamic piston-shock relationship.

also carried nonthermal particles, consistent with the scenario that the plasmoid is the heated prominence material (see, e.g., Wagner, 1984). Presence of nonthermal electrons can also be inferred occasionally from hard X-rays (Hudson et al., 2001). Recently, Nitta and Akiyama (1999) looked for X-ray ejecta in 17 limb flares and compared them with LASCO data. They found that (i) flares not associated with CMEs also lacked X-ray ejections, and (ii) the X-ray ejecta were inner structures of CMEs. These results are consistent with the dense prominence material present in the core of CMEs. To be "visible" in X-rays, they must have been heated. However, frontal structure of CMEs can also be occasionally seen in X-rays, as was reported by Gopalswamy et al. (1996). Spectroscopic observations also confirm that the prominence core can be hot (Ciaravella et al., 2003).

6.5 CMEs and Radio Bursts

Moving type IV bursts indicate magnetized plasma ejection; type II bursts indicate superAlfvenic mass motion. Therefore, these two bursts are expected to be closely related to CMEs. Moving type IVs come in three varieties: advancing fronts, expanding arches and isolated plasmoids (see Stewart, 1985 for a review). The isolated sources originate from the heated prominence material, also detected in X-rays and EUV. The advancing fronts and expanding arches must be structures associated with the CME itself (Gopalswamy and Kundu, 1989; Bastian et al., 2001), "visible" because of the nonthermal electrons trapped in them. The nonthermal electrons may be accelerated at the reconnection site beneath the CMEs or by the shock ahead of the CME.

Coronal and interplanetary shocks are inferred from metric and longer wavelength type II radio bursts, respectively (Wild et al, 1950; Malitson et a., 1973). Gosling et al. (1976) found that $\sim 85\%$ of CMEs with speed > 500 km s^{-1} were associated with type II and/or type IV bursts. In a

reverse study, Munro et al. (1979) found that almost all type II or type IV bursts originating from within 45° of the limb were associated with CMEs. The speed distribution of coronal shocks was found to be similar to that of CMEs associated with type II bursts (Robinson, 1985). These observations clearly were consistent with the idea that CMEs moving faster than the local Alfven speed can drive an MHD shock. Later observations indicated metric type II bursts without CMEs and fast CMEs without metric type II bursts (Sheeley et al., 1984; Kahler et al., 1984, 1985). From these results it was inferred that some of the coronal shocks may be flare blast waves, consistent with the type II source location behind the leading edge of CMEs (Wagner and MacQueen, 1983; Gary et al., 1984; Robinson and Stewart, 1985; Gopalswamy et al., 1992).

Using Solwind (coronagraph) and Helios (in situ) data, Sheeley et al. (1985) found a near one-to-one correspondence between CMEs and IP shocks. All kilometric type II bursts observed by ISEE-3 are known to be associated with fast (> 500 km s^{-1}) and energetic CMEs and IP shocks (Cane et al., 1987). Recent data from Wind/WAVES (Bougeret et al., 1995) indicate that all decameter-hectometric (DH) type II bursts (1-14 MHz) are also associated with fast and wide CMEs capable of driving shocks (Gopalswamy et al., 2001b). Can we extend this CME-type II connection to metric type II bursts also? There are several arguments in favor of the idea that even metric type II bursts are due to CME-driven shocks: 1. Type II bursts without associated CMEs have been revisited by Cliver et al. (1999) to show that the CMEs might have been missed due to observational constraints. Further evidence came from a comparison of metric type II bursts with LASCO/EIT data: while no white-light CMEs were observed for some metric type II bursts, there were EUV eruptions from close to the disk center (Gopalswamy et al., 2001a), suggesting that these CMEs may have been masked by the occulting disk. 2. Lara et al. (2003) studied the CME properties of (i) metric type II bursts with no IP counterparts and (ii) IP type II bursts at frequencies $\leq$14 MHz. They found that the speed, width and deceleration of CMEs progressively increased for the general population of CMEs, CMEs associated with metric type II bursts and CMEs associated with IP type II bursts, in that order. This is clear evidence that the energy of a CME is an important factor in deciding whether it will be associated with a type II burst, consistent with an earlier conclusion by Robinson (1985) when comparing speeds of CMEs associated with metric type II bursts and those of IP shocks associated with km type II bursts. 3. The type II burst association with low-speed (200 km s^{-1}) CMEs and the lack of it for a large number of fast (speed > 900 km s^{-1}) and wide ($> 60°$) CMEs can be explained as a direct consequence of the Alfven speed profile in

the ambient medium (Gopalswamy et al., 2001a). 4. The difference in drift rates of type II bursts below and above 1 MHz (Cane, 1983) and the lack of correlation between speeds derived from metric type II bursts and associated CMEs (Reiner et al., 2001) can be explained if we note that the CME speed changes rapidly in the inner corona and the CME is propagating through the region of highly variable Alfven speed. 5. The positional mismatch between CME leading edge and type II bursts can be explained by the preferential electron acceleration in the quasiperpendicular region of the CME bow shock (Holman and Pesses, 1983). 6. A blast wave is expected to be without a driver, but there is no evidence from in situ data for a shock without a driving ejecta. Almost all IP shocks followed by ICMEs seem to have a piston-shock relationship (see Fig. 15), and the corresponding white-light CMEs can be identified. Shocks detected "without drivers" can be attributed to limb CMEs so they are also driven, but only the flanks arrive at Earth (Schwenn, 1996; Gopalswamy et al., 2001a). It appears that all type II bursts can be associated with CMEs if we consider the combination of CME characteristics (speed, width) and the Alfven speed profile in the ambient medium.

The advent of EIT waves (Thompson et al., 1999) has provided some additional input to the problem of coronal shock source. Based on the good correspondence between EIT waves and metric type II bursts, Mann et al. (1999) suggested that EIT waves are of flare origin and might be the pre-shock stage of coronal shocks inferred from metric type II bursts. However, Gopalswamy and Kaiser (2002) pointed out that a CME-driven shock can form low in the corona where the Alfven speed is < 300 km s^{-1} and hence explain the metric type II burst and even the subsequent IP type II burst. One class of EIT waves known as "brow waves" (owing to their arc-like appearance in EIT images, - see Gopalswamy, 2000; Gopalswamy and Thompson, 2000) are spatially and temporally coincident with metric type II bursts (Gopalswamy et al., 2000d). Biesecker et al. (2002) later classified the brow waves as "events with sharp brightenings" and found them to be associated with metric type II bursts, flares, and CMEs. They also found an unambiguous correlation between EIT waves and CMEs, but a significantly weaker correlation between EIT waves and flares. There were also attempts to interpret wavelike features in soft X-ray images to be blast waves and associate them with Moreton waves (Moreton, 1960) and metric type II bursts (Narukage et al., 2002; Hudson et al., 2003). However, both of these reports did not take the presence of CMEs into consideration. For example, in the 1998 May 06 event at 08:03 UT studied by Hudson et al. (2003), there was also a 1100 km s^{-1} CME (see Table 1 Gopalswamy,

2003a), whose onset preceded the type II burst and hence cannot be ruled out as the source of the metric type II burst. It is quite likely that the EIT waves (at least the brow type) are coronal counterparts of Moreton waves, but are not inconsistent with a CME source. While we cannot completely rule out the possibility of flare blast waves causing metric type II bursts, the available and new evidence seem to favor CME-driven shocks (see also Mancuso and Raymond, 2004). Unfortunately, there is no reliable way of directly detecting shocks in the corona, except for possible shock signatures observed by UVCS (Raymond et al., 2000) and the white-light shock signatures (Sheeley et al., 2000; Vourlidas et al., 2003), which are not without CMEs.

6.6 CME Interaction and Radio Emission

Given the high rate ($\sim$ 6/day) of CME occurrence during solar maximum and the observed range of speeds, one would expect frequent interaction between CMEs. Although interactions among shocks and ejecta are known to happen in the heliosphere (Burlaga et al., 1987), SOHO images combined with the Wind/WAVES dynamic spectra provided direct evidence for CME interactions very close to the Sun (Gopalswamy et al., 2001c; 2002a). These interactions resulted in broadband nonthermal radio enhancements in the decameter-hectometric (DH) wavelength domain. Strengthening of shocks when propagating through the dense parts of preceding CMEs and trapping of particles in the closed loops of preceding CMEs were suggested as possible mechanisms that increase the efficiency of particle acceleration (Gopalswamy et al., 2002b). Shock strengthening can be seen from the fact the change in local Alfven speed (Va) is related to density (n) and magnetic field (B) changes: $dVa/Va = dB/B - (1/2)dn/n$. Recent numerical simulations support such shock strengthening (Wu et al., 2002). A shock traveling through a denser medium would be locally stronger and would accelerate more electrons resulting in enhanced radio emission, provided the magnetic field does not change significantly.

Figure 16 illustrates a recent CME interaction event: A sudden radio enhancement occurred over an existing Wind/WAVES type II radio burst on 2003 November 4. The radio enhancement is brighter than the associated type II burst and hence is nonthermal in nature. A very fast, shock-driving CME (CME2, 2657 km s^{-1}) approached a slower CME (CME1, $\sim$1000 km s^{-1}) and its dense core (CORE1, $\sim$700 km s^{-1}). The radio enhancement occurred when CME2 reached a heliocentric distance of 18 $R_\odot$, close to the core of CME1. The 21:18 UT SOHO image shows that the CME2 and CORE1 are very close when the ra-

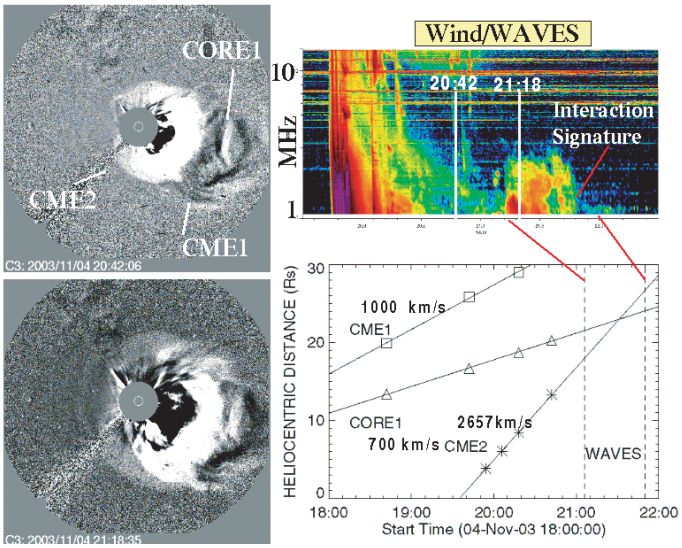

Figure 8.16. Wind/WAVES dynamic spectrum (top right) showing the interaction signature and the height-time diagram (bottom right) of the 2003 November 04 CMEs. The first CME (CME1), its core (CORE1) and the second CME (CME2) are marked in the SOHO image at 20:42 UT (top left). The SOHO image at 21:18 (bottom left) was taken when the Wind/WAVES interaction signature in radio was in progress. The times of the two SOHO images are marked on the WAVES dynamic spectrum. The duration of the interaction signature is denoted by the two vertical dashed lines on the height-time plot. The speeds of CME1, CME2, and CORE1 are also shown.

dio enhancement started. The radio emission lasted for about 40 min, roughly the time taken by the CME-driven shock to traverse CORE1 (size $\sim 7\ R_{\odot}$). The high frequency edge of the type II burst was at ~ 1 MHz when the interaction signature started with a high-frequency edge of 3 MHz. A jump of 2 MHz in frequency would correspond to a density jump of 4 with respect to the ambient corona. This is also consistent with the relatively high white-light brightness of CORE1. The same interaction signature was observed by radio receivers on board Ulysses and CASSINI, which were at distances of 5 and 8.7 AU, respectively. The signatures arrived at CASSINI and Ulysses with a delay corresponding to the light travel times. Wind, Ulysses, and CASSINI were widely separated in heliocentric distance as well as angular separation, suggesting that the interaction signature is not narrowly beamed.

7. CMEs and Solar Energetic Particles

Kahler et al. (1978) found CMEs to be necessary requirements for the production of SEPs and hence suggested that SEPs may be accelerated

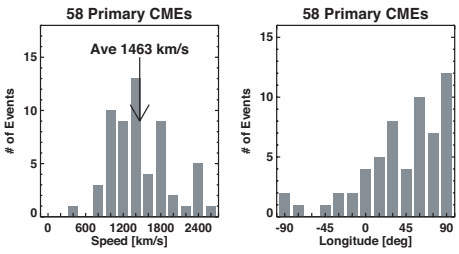

Figure 8.17 Distributions of speed (left) and source longitudes of CMEs associated with 58 major (proton intensity exceeding 10 particles per (cm^2 s sr)) SEP events from the period 1996-2002. The 90° bins also contain events from behind the limb.

by the shocks ahead of CMEs. The current paradigm is that impulsive, short-lived SEP events are due to flares and the large, gradual, long-lived events are accelerated in CME-driven shocks (see, e.g. Lin, 1987, Reames, 1999). Recent data also indicate that large SEP events are invariably associated with fast and wide CMEs (Fig. 17). CMEs from the western hemisphere typically result in high SEP intensity at Earth due to better connectivity (see Fig. 17), although it is not uncommon for CMEs from the eastern hemisphere to result in SEP events at Earth. Despite the general acceptance of CME-driven shocks as the source of large SEP events (Lee, 1997; Reames, 1999; Tylka, 2001), there is still no widely accepted theory that explains all the observed properties of SEPs. For example, the CME speed and SEP intensity are reasonably correlated, yet the scatter is very large (see Fig. 18): for a given CME speed, the SEP intensity has been found to vary over four orders of magnitude (Kahler, 2001; Gopalswamy et al., 2003c) with no satisfactory explanation. However, the SEP intensity is better correlated with the CME speed than with the flare size (Fig. 18).

A Type II burst is the primary indicator of shock near the Sun, where the SEPs are released (a few $R_\odot$ from the Sun - see, e.g., Kahler, 1994). The DH type II bursts also originate from this region and are known to have a 100% association with SEP events (Gopalswamy, 2003a). The occurrence rates (per Carrington Rotation) of large SEP events (>10 MeV protons from GOES), fast and wide CMEs from the frontside western hemisphere, IP shocks (detected in situ), DH type II bursts and major (GOES M and X-class) flares are quite similar, except for major flares, of which there were too many (Gopalswamy et al., 2003b,c). The close correlation among all these phenomena suggests that CME-driven shocks accelerate electrons (to produce type II bursts) and protons (detected as SEP events).

The simple classification of impulsive and gradual SEP events has recently been brought into question. Most of the CMEs associated with large SEP events are also associated with intense flares, so it is often dif-

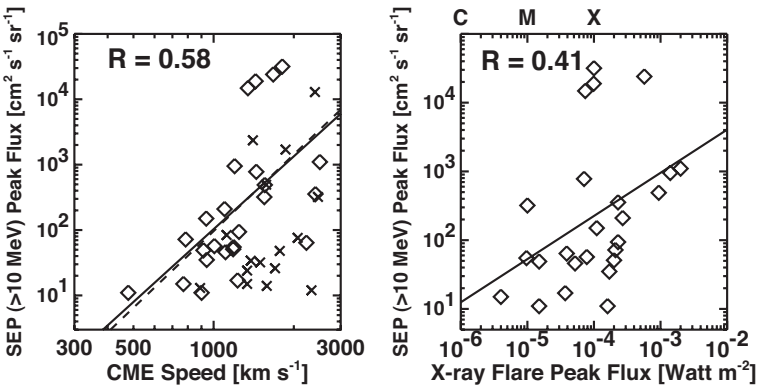

Figure 8.18. Scatter plot of the SEP intensities of > 10 MeV proton events with (left) CME speeds and (right) X-ray flare size. All events are plotted in the left panel, but only the 25 events with 0° < longitude < 90° (diamonds) are included in the correlation. The solid lines are best fits to the diamonds. The correlation coefficients are r=0.58 for CME speeds (confidence level 99.9%) and 0.41 for X-ray flux (confidence level 98%). Excluding the outlier CME with a speed of 478 km s^{-1} results in r=0.54 (confidence level 99.75%) and the dashed line. See Gopalswamy et al. (2003c for details.

ficult to untangle the contributions from flare and shock sources (Cliver, 1996; Kocharov and Torsti, 2002). Flare particles (Mason et al., 1999) or SEPs from preceding CMEs (Kahler, 2001) may form seed particles for CME-driven shocks near the Sun as well as at 1 AU (Desai et al., 2003). Long rise times of some SEP events seem to be due to successive SEP injections (Kahler, 1993). SEP-producing shocks seem to propagate through the corona with preceding CMEs (Gopalswamy et al., 2002a). Large SEP events with preceding wide CMEs within a day from the same active region tend to have higher intensity (Gopalswamy et al., 2003c). Multiple shocks and CMEs can form configurations that can enhance the SEP intensity significantly (Kallenrode and Cliver, 2001; Bieber et al., 2002). Thus, the presence of preceding CMEs means disturbed conditions in the coronal and IP medium through which later CMEs propagate: density, flow velocity, magnetic field strength, magnetic field geometry, and solar wind composition may be different compared to normal solar wind conditions. Accelerated particles propagating through a medium denser than the normal solar wind (due to a preceding CME) may affect the observed charge states of the ions if the product of the density and the residence time is large enough to allow for additional electron stripping (Reames et al., 1999; Barghouty and Mewaldt, 2000).

8. CMEs in the Heliosphere

While the existence of magnetized plasma clouds was contemplated in the 1950s, their detection became possible with space borne measurements (Burlaga et al., 1981, Lepping et al., 1990). Helios 1 detected a magnetic loop behind an IP shock, which Burlaga et al. (1981) defined as a magnetic cloud (MC). The connection between CMEs and MCs was recognized when a Helios 1 MC was related to a white-light CME that left the Sun two days before (Burlaga et al., 1982). Analyzing the helium abundance enhancements (HAEs - Hirshberg et al., 1972) in the high speed plasmas behind IP shocks, Borrini et al. (1982) concluded that the HAEs must be the IP signatures of CMEs. At present a large number of IP signatures are used to identify the CME-related plasmas in the solar wind (see, e.g. Gosling et al., 1990): bidirectional streaming of superthermal electrons and ions, unusual abundances and charge states, low electron and proton temperatures, strong magnetic fields with flux rope structures, and Forbush decreases. It must be noted that not all of the signatures are present in all events (see Neugebauer and Goldstein, 1997). CMEs in the solar wind are commonly referred to as 'ejecta' or interplanetary CMEs (ICMEs). In situ observations of CMEs can be used to infer the magnetic field topology of the ICMEs and the physical conditions of their birthplace near the Sun (see, e.g., Henke, 1998; Lepri et al., 2001). When a CME moves past a spacecraft in the solar wind, the following sequence of structures would be detected: IP shock, sheath, and ejecta. On rare occasions, one observes cool dense material towards the end of the ejecta that resemble the prominence resting at the bottom of the coronal cavity in the pre-eruption phase of CMEs (Burlaga et al., 1998; Gopalswamy et al., 1998). As a working hypothesis, one can relate CMEs and ICMEs as follows: CME shock $\rightarrow$ IP shock, CME front $\rightarrow$ sheath, CME void $\rightarrow$ ICME (or ejecta), and CME core $\rightarrow$ density pulse (Gopalswamy, 2003b). Cliver et al. (2003) estimated that Earth is embedded within CME-related flows (shocks, sheaths and ejecta) for $\sim 35\%$ of the time during solar activity maximum and $\sim 10\%$ of the time during solar minimum. Only those CMEs, which originate close to the Sun center (within 30°) are intercepted by Earth as ICMEs (Gopalswamy, 2002). Using bidirectional electron signatures, Gosling et al. (1992) found ~ 72 (8) ICMEs/year during solar activity maximum (minimum), similar to the variation in CMEs discussed in section 4. Klein and Burlaga (1982) found that $\sim 33\%$ of ICMEs were MCs. Recent studies show that the fraction of ICMEs that are MCs ranges anywhere from 11% to 100% (Cane and Richardson, 2003; see also Table 1 of Gopalswamy et al., 2000a).

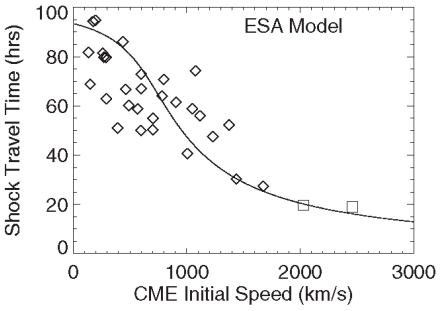

Figure 8.19 The empirical shock arrival (ESA) model, which predicts the shock travel time based on the initial speed of CMEs in the sky plane. The diamonds are for shocks driven by magnetic clouds. The squares represent the two fastest shocks of cycle 23, which originated from the ultrafast CMEs on 2003 October 28 (11:06 UT, 2459 km s^{-1}) and 2003 October 29 (20:41 UT, 2029 km s^{-1}).

ICMEs are responsible for the severest of geomagnetic storms and can be directly related to front-side halo CMEs (Gosling, 1993; St. Cyr et al., 2000). Webb (2002) finds that the fraction of halos associated with geomagnetic storms considerably decreased towards solar maximum. For example, 92% of the halos were associated with geomagnetic storms in the year 1997, while the fraction dropped to 35% in the year 2000. Detailed information on the internal structure (e.g., whether it contains southward magnetic field component) of halo CMEs is needed to understand why only certain halo CMEs result in geomagnetic storms. Thus the travel time of CMEs to 1 AU and their geoeffectiveness (magnitude and duration of geomagnetic storms) are of practical importance for space weather applications. Availability of simultaneous data on CMEs and ICMEs has made it possible to establish a relationship between their speeds (Lindsay et al., 1999). Influence of the solar wind on CMEs as they propagate away from the Sun can be postulated as an average IP acceleration (Gopalswamy et al., 2000a), which can be used to predict the travel time of CMEs (Gopalswamy et al., 2001e; Gopalswamy 2002) and shocks (Gopalswamy et al., 2003d) to various points in the heliosphere. Figure 19 shows the empirical shock arrival (ESA) model curve with observed travel times of MCs of cycle 23. The empirical model helps us understand the gross propagation of Earth-directed CMEs originating close to the disk center (within $\pm 30^{\circ}$) and propagating through quiet solar wind. Drastically different conditions such as high speed wind, preceding CMEs (Manoharan et al., 2004) and significant projection effects (Gopalswamy et al., 2000b; Michalek et al., 2003) may also affect the predicted shock arrival times. As for geoeffectiveness, the ICME has to have southward magnetic field component, which is a difficult problem.

There have been several attempts to relate the magnetic field structure of the ejecta to that of filaments (e.g., Bothmer and Schwenn, 1994; Marubashi, 1997; Bothmer and Rust, 1997), arcades overlying filaments (Martin and McAllister, 1997), and the overlying global dipolar field of the Sun (Crooker 2000; Mulligan et al., 1998). However, there is no systematic scheme to predict the internal structure of an ICME based on magnetograms of the eruption regions.

8.1 High Latitude CMEs

Motion of magnetic clouds can continue in the heliosphere (Yeh, 1995) and has been observed beyond 11 AU (Burlaga et al., 1985; Funsten, et al., 1999), which means these objects must be commonplace in the heliosphere. While Voyager observations provided information on the heliospheric CMEs (HCMEs) in the ecliptic plane, high-latitude CMEs were first observed in situ by Ulysses (Gosling et al, 1994; Gosling and Forsyth, 2001). Ulysses CMEs observed during minimum conditions were fast compared to the ones observed during maximum conditions. A new class of CMEs known as "over-expanding" CMEs were discovered by Ulysses (Gosling et al., 1994). These CMEs have high internal pressure drive shocks due to the expansion into the heliosphere, rather than from the motion away from the Sun. Based on Ulysses observations (heliocentric distance 5.3 - 3.0 AU) over a 16-month interval at latitudes S30-S75, Gosling and Forsyth (2001) found that the HL HCMEs have an average duration of $\sim$67 h and a radial size of $\sim$0.7 AU (compared to the 0.25 AU at 1 AU); the occurrence rate of 15 per year is about 5 times smaller than the ecliptic rate at 1 AU. The ratio of HL to LL HCMEs seems to be very similar to the overall ratio ($\sim$ 20%) with a slightly different definition of HL (latitude $\geq 60^\circ$) and LL (latitude $< 60^\circ$) CMEs (Gopalswamy et al., 2003e).

Since the latitudes of CMEs are derived from the central position angle of CMEs in the sky plane, Gopalswamy et al. (2003e) considered HL CMEs as those with latitude $\geq 60^\circ$, and the LL CMEs with latitudes $\leq 40^\circ$. With this definition, they obtained a HL-to-LL CME ratio of 25%. To be consistent with this definition, we compared the Ulysses and SOHO/LASCO CMEs for the period July 10, 2000 to February 5, 2001, when Ulysses was poleward of S60. During these seven months, Ulysses detected 8 HCMEs, giving rate of 13.7 per year, very similar to Gosling and Forsyth's rate. Over the same interval, SOHO/LASCO observed 101 CMEs poleward of S60 and 602 LL CMEs, giving an HL-to-LL ratio of $\sim$17%. Interestingly, the ratio of HL CMEs at the Sun and HCMEs at Ulysses is $\sim$8%. The ratio of LL CMEs (602) at the Sun

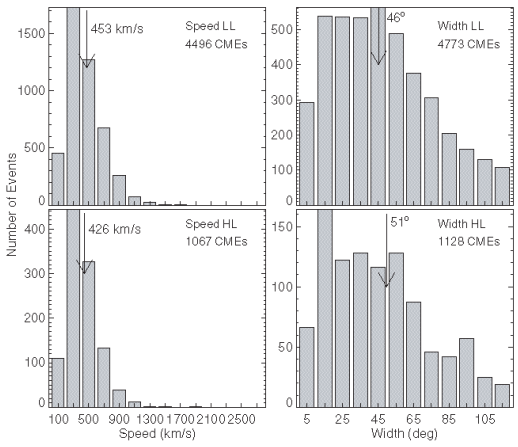

Figure 8.20 The speed and width distributions of high-latitude ($\geq 60°$, HL) and low-latitude ($\leq 40°$, LL) CMEs, with average values marked. CMEs with latitudes between 40 and 60° are not included for a clear separation between the two populations. CMEs with widths $\geq 120°$ are excluded because it is difficult to obtain their latitudes. The distributions of HL and LL CMEs are not very different.

to the ICMEs at 1 AU (25, see Cane and Richardson, 2003) is ∼4%, which becomes ∼8% if we assume that half of the SOHO LL CMEs are backsided. Figure 20 shows the overall comparison between HL and LL CMEs for the entire cycle 23 until August 2003. The HL-to-LL ratio (∼14%) is not too different from the numbers above. Although these comparisons indicate that the latitudinal distribution of CMEs at the Sun and in the heliosphere may be similar, Reisenfeld et al. (2003) reported that two of the equatorial CMEs observed by SOHO/LASCO were observed at Earth as well as by Ulysses at high latitudes (above N75). The large separation between Earth and Ulysses in latitude (73°) and longitude (64°) for one of the events is consistent with the large width of some white-light CMEs (>120°). However, these huge events are rare at the Sun.

9. CMEs and Solar Polarity Reversal

Two magnetic cycles have been completed since Horace Babcock first noted the reversal of polarities of solar polar magnetic fields in 1959 (cycle 19). The Sun faithfully reversed the sign of its polar magnetic fields during all the sunspot cycles (20-23) since then. Common signatures of magnetic polar reversals on the Sun are the disappearance and reformation of polar coronal holes (Webb, et al., 1984; Bilenko, 2002; Harvey and Recely, 2002) and the disappearance of the polar crown filaments (PCFs) following a sustained march to the poles (Waldmeier, 1960; Cliver et al., 1994; Makarov, Tlatov, and Sivaraman, 2001). Studying the polarity reversals of cycle 23, Gopalswamy et al. (2003e) found that the epochs of solar polar reversal are closely related to the cessation of HL CME activities, including the non-simultaneous reversal in the north and south

poles (see Fig. 21). Before complete reversal, several temporary reversals take place with corresponding spikes in the HL CME rates. The high-latitude CMEs also provide a natural explanation for the disappearance of closed field structures that approach the poles, which need to be removed before the reversal could be accomplished. The polarity reversal seems to be a violent process involving CMEs of mass a few times 10^{15} g and a velocity of hundreds of km s^{-1}. The kinetic energy of each of these CMEs is typically a few times 10^{30} erg. Figure 20 shows that there were $\sim 10^3$ HL CMEs over a period of $\sim 10^3$ days, during which the reversal was completed. This amounts to an energy dissipation rate of $\sim 10^{30}$ erg/day. The results presented here also support the hypothesis that CMEs may represent the process by which the old magnetic flux and helicity are removed and replaced by the those of the new magnetic cycle (Low 1997; Zhang and Low, 2001). Inclusion of CMEs along with the photospheric and subphotospheric processes completes the full set phenomena that need to be explained by any successful theory of the solar dynamo.

10. CMEs and Cosmic Ray Modulation

Newkirk et al. (1981) identified CMEs as the solar origin of the low-frequency power in the interplanetary magnetic field fluctuations and suggested that the solar cycle dependent modulation of galactic cosmic rays (GCRs) can be explained by the presence of CME-related magnetic inhomogeneities in the heliosphere. Although they explored CMEs at latitudes below 60°, we now know that CMEs are present at all latitudes at least during solar maximum as isolated (Gosling and Forsyth, 2001; Balogh, 2002) or as merged interaction regions (Burlaga et al., 1993). The relationship recently found between HL CMEs and the reversal of global solar magnetic field (Gopalswamy et al., 2003e), and the relationship of the latter with the drift of GCRs into the solar system (Jokipii et al., 1977), suggest that HL CMEs may play an important role in long-term GCR modulation. SOHO results have conclusively shown the existence of a higher and more cycle-dependent CME occurrence rate (varying by factors up to 10) than pre-SOHO data indicated (Wagner, 1984). It was recently found that the inverse of the GCR intensity was correlated well with the HL CME rate during the rise phase of cycle 23 (Lara et al., 2004). This provides a clue to the 22-year pattern of GCR modulation, which does not directly follow solar activity indices such as SSN (see, e.g., Potgeiter et al., 2001). As we pointed out before, CME rate need not follow SSN, owing to the PCF-related CMEs,

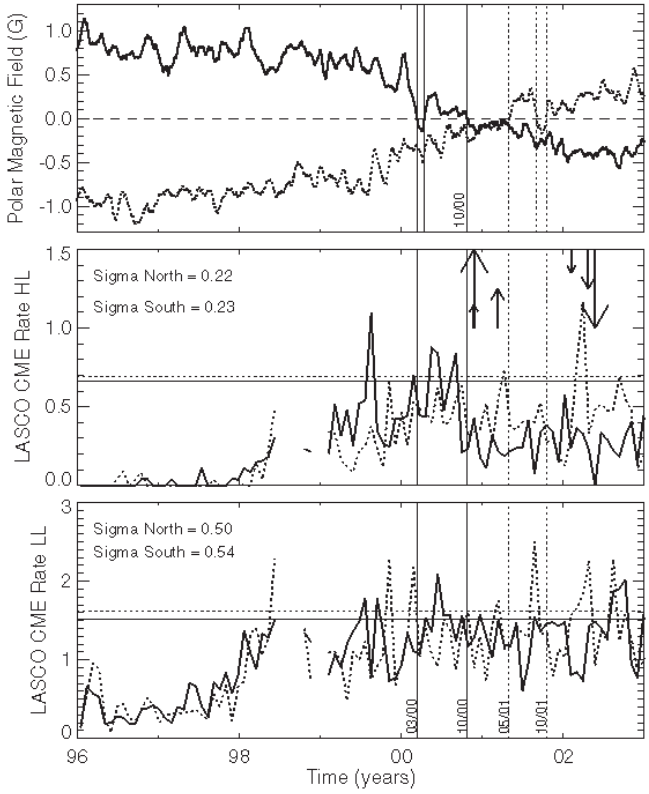

Figure 8.21. (top) The polar field strength averaged over regions poleward of 70° (from NSO/Kitt Peak). Times of polarity reversal are marked by the vertical lines (solid -north; dashed - south). CME rates from high (middle) and low (bottom) latitudes are distinguished by the hemispheres (solid - north and dotted - south). Times when the PCF branch disappeared are marked by small (Lorenc et al., 2003) and medium (Harvey and Recely 2002) arrows. Large arrows mark the times of cessation of high latitude prominence eruptions from Fig. 20. The direction of the arrows indicates the hemisphere (up - north; down - south). The horizontal lines in the middle and bottom panels show the 3-sigma levels of the CME rates (solid - north; dotted - south). The standard deviation (sigma) of the rates in the north and south are marked in the respective panels.

so treating the HL and LL CMEs separately may help understand the GCR modulation pattern.

The drift of positively-charged GCRs in the solar system is known to be poleward when the polarity at the solar north pole is positive (known as A>0 cycle) and equatorward when the solar polarity is negative (A<0 cycle). The poleward and equatorward approaches are switched for the negatively charged GCRs such as electrons and antiprotons (Bieber et

al., 1999). The A>0 and A<0 epochs commence when polarity reversal completes during even and odd numbered solar activity cycles, respectively. For example, there was a switch from A>0 to A<0 in the first half of 2002. This preferential direction of approach of GCRs immediately suggests that HL and LL CMEs should be alternately important for blocking GCRs during the A>0 and A<0 cycles. During A>0 cycles, GCR ions enter the heliosphere from the polar direction, so the HL CMEs must be effective in blocking them. For A<0 cycles, the approach of GCR ions is equatorward, so LL CMEs effectively block them. In order to see this effect, we compared the GCR intensity (from Climax neutron monitor) and HL and LL CME rates for the declining phase of cycle 21 (after the start of the A<0 epoch) and the rising phase of cycle 23 (before the end of the A>0 epoch). For these two phases, complete CME observations exist and the CME rates can be easily separated into LL and HL parts (Gopalswamy et al., 2003e). Figure 22 shows two cross-correlation plots comparing GCR intensity and HL and LL CME rates averaged over Carrington Rotation (CRot) periods (27.34 days). The cycle 21 data are somewhat noisy because the CME data were obtained with lower sensitivity compared to the SOHO/LASCO data for cycle 23. Nevertheless one can clearly see that the roles of HL and LL CMEs are reversed in the two epochs: higher anticorrelation was obtained between GCR intensity and LL CMEs for the A<0 epoch. On the other hand, the GCR intensity showed a better anticorrelation with the HL CME rate for the A>0 epoch. The tandem influence of HL and LL CMEs is thus consistent with the 22 year modulation cycle of GCRs.

On the basis of the above discussion, we can provide a tentative explanation as to how the GCRs and CMEs are coupled, as follows. An A>0 cycle begins right after the completion of the polarity reversal during the maximum of an even-numbered cycle. GCRs start entering the heliosphere from the poles. Since HL CMEs have subsided around this time (Gopalswamy et al., 2003e), the GCR intensity recovers quickly, reaching peak intensity at the solar minimum, when the new odd-numbered cycle begins. As the solar activity builds up, LL CMEs become more abundant, but there are no HL CMEs during the rise phase so GCR intensity is still relatively high. When HL CMEs start appearing in the pre-maximum phase of the odd cycle the GCR intensity drops precipitously until the solar polarity reverses at the odd-cycle maximum to begin the A<0 epoch. In the A<0 epoch, GCRs start entering equatorward. Since the LL activity during the declining phase is relatively high, GCR intensity continues to be affected by the LL CMEs until the activity approaches the activity minimum. Then comes the rise phase of the next even cycle, with continued blocking of GCRs solely by LL

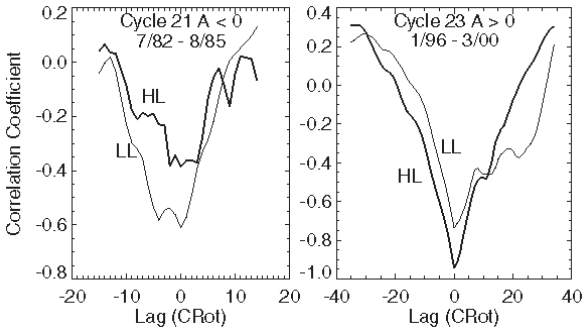

Figure 8.22 Cross-correlation between GCR intensity and HL and LL CME rates for (left) the A<0 epoch of cycle 21 and (right) the A>0 epoch of cycle 23.

CMEs. The appearance of HL CMEs before the maximum of the even cycles is of no consequence because the GCRs still approach equatorward and hence severely affected by the LL CMEs of the even-numbered cycle. This completes the 22-year cycle consisting of flat-topped and pointy components. The pointy component is tightly correlated with SSN (because of modulation by LL CMEs); the flat-top component is correlated with HL CMEs (PCF-related) owing to their appearance just before the solar maximum. The flat-topped response naturally explains the lag between solar activity and GCR recovery (Cliver and Ling, 2001).

11. Some Outstanding Questions

11.1 CME Initiation

Even after three decades of CME observations, we do not fully understand how CMEs are initiated. We do understand the details of the pre-CME structure: a set of one or more closed flux systems that eventually erupt. This could be a simple bipole with a core-envelope structure (Moore et al., 2001; Magara and Longcope, 2001), a flux rope with overlying restraining field (Low and Zhang, 2002; Forbes et al., 1994; Linker et al., 2001; Wu et al., 2000), a combination of bipoles (Machado et al., 1988) or multipolar structure (Antiochus et al., 1999; Chen and Shibata, 2000; Feynman and Martin, 1995). A successful CME model should account for the observed range of speed, mass, acceleration of CMEs, and the distribution of energy into heating, particle acceleration and mass motion. The current level of sophistication of CME models is less than adequate to account for all the observed characteristics (see e.g., Forbes, 2000; Klimchuk, 2000). Initial models based on the assumption of flare-produced CMEs (e.g., Dryer, 1982) have largely been abandoned because CME onset precedes flare onset (e.g., Wagner et al., 1981). After this, the emphasis shifted to loss of equilibrium (Low, 1996), primarily motivated by the three-part structure (frontal structure, cavity, and core) of CMEs and the coronal helmet streamers well observed in eclipse pic-

tures (Saito and Tandberg-Hanssen, 1973). The cavity is identified as a flux rope of low plasma density and high magnetic field strength. In the pre-eruption state, the flux rope is held down by the prominence mass, the mass of the plasma contained in the overlying fields, and the magnetic pressure of these overlying fields. A CME is produced when the confinement of the flux ropes breaks down for a variety of reasons, such as loss of prominence mass (Low and Zhang, 2002). The interaction between the current in the flux rope and in the current sheets in the overall configuration decides the eruption and dynamics of the flux rope. This way, it is even possible to account for the accelerating CMEs from inverse polarity prominences and the constant speed CMEs from normal polarity prominences.

It is currently believed that the energy required to propel the CME has to come from the magnetic fields of the solar source region (see, e.g., Forbes, 2000). To illustrate the maximum energy that may be needed in CMEs, let us consider the 2003 November 04 CME, the fastest ($\sim$2700 km s^{-1}) event of cycle 23 (see Fig. 12): The CME had a mass of $\sim 2\times10^{16}$g, so that we can estimate the kinetic energy to be $\sim7\times10^{32}$ erg. There is probably no other CME with an energy larger than this, so we can take that the largest energy released from an eruption is $\sim 10^{33}$ erg, and might represent the maximum free energy in the magnetic fields of the source. Considering a large active region (photospheric diameter $\sim$5 arcmin), we can estimate its coronal volume of 10^{30} cm^3. An average coronal field of 200 G over this volume implies a magnetic potential energy of $\sim 10^{33}$ erg. Microwave observations of the corona above sunspots have shown magnetic fields exceeding 1800 G (White et al., 1991), so an average of 200 G is not unreasonable. The highest value of potential magnetic energy in active regions surveyed by Venkatakrishnan and Ravindra (2003) is also $\sim 10^{33}$ erg. Since the potential magnetic energy is probably smaller than the total magnetic energy by only a factor $<$2 (Forbes, 2000), we infer that occasionally a substantial fraction of the energy contained in an active region may be released in the form of a CME. How this much free energy builds up in active regions is not fully understood.

11.2 How do CMEs Evolve?

In section 8, we saw that only a small fraction of CMEs originating at the Sun seem to reach 1 AU and beyond. This means a large number of CMEs may not survive as distinct entities for too long. Figure 23 shows the evolution of a white-light CME, which faded within the LASCO/C2 FOV above the northeast limb. The final height up to which the CME

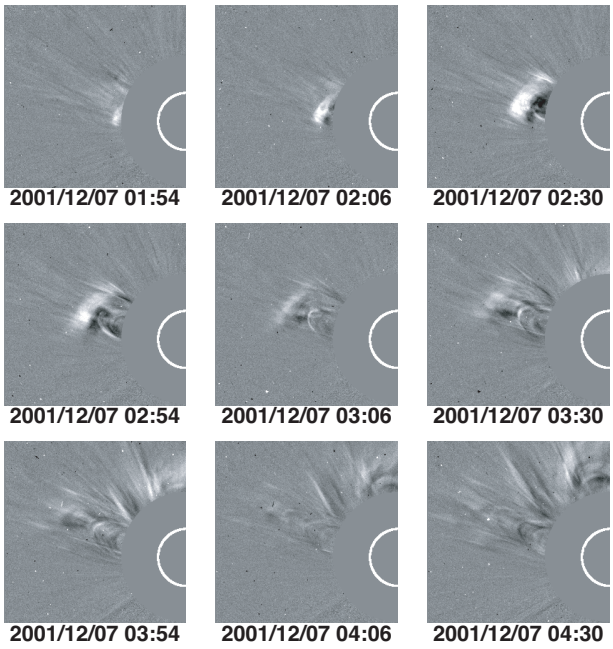

Figure 8.23. Evolution of the 2001 December 07 CME at 01:54 UT as observed by SOHO/LASCO from the above the northeast limb. The CME is well defined but within an hour falls apart and fades away.

could be tracked was $\sim$ 5.5 $R_\odot$. The CME was slow (273 km s^{-1}) and did not show deceleration. Figure 24 shows the distribution of the final heights of all the CMEs within the $32R_\odot$ FOV of LASCO. Clearly, many CMEs could not be tracked beyond $\sim 10R_\odot$. It is not clear if these CMEs faded because their density became too small to be detected or they ceased to exist as an entity different from the solar wind. The distribution also shows a second peak close to the edge of the field of view. Preliminary investigation shows that these are indeed the fast and wide CMEs (including halo CMEs). What causes the rapid dissipation of the smaller CMEs? Speculations such as the presence of enhanced turbulence in the 10-20 $R_\odot$ region (Mullan, 1997) need to be explored to understand them.

The shock-driving CMEs constitute a small fraction (a few percent) of all CMEs (Gopalswamy et al., 2003c), much smaller than the 20% estimated by Hundhausen (1999). The majority of CMEs are likely to be subAlfvenic and supersonic. These CMEs must be driving slow and intermediate shocks, as suggested by simulation studies (Whang, 1987; Steinolfson, 1992). Flat-top and concave upward morphology observed

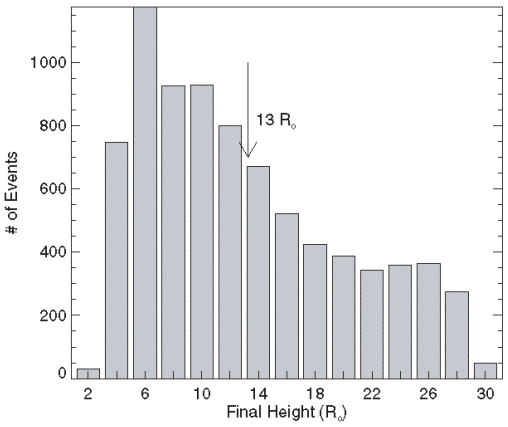

Figure 8.24 Distribution of the final heights of all the LASCO CMEs from 1996 to 2003. The average value is only 13 $R_\odot$, compared to the LASCO FOV of $32R_\odot$. Note the second peak in the distribution close to the edge of LASCO FOV. The second bin from the left corresponds to the edge of the LASCO/C2 FOV. The large number in this bin is likely due to the fact that many CMEs could not be tracked from C2 to C3 FOV.

in some SMM CMEs are thought to indicate the presence of slow and intermediate shocks (Hundhausen 1999). The extensive SOHO database needs to be exploited to fully understand the slow and fast mode shocks. Such studies will be helpful in understanding the lateral structure of CMEs.

CMEs are observed as density enhancements within the coronagraph field of view. On the other hand there are many in situ signatures of CMEs as discussed in section 7. Most models dealing with CME initiation assume that the CME is a flux rope coming out of an eruption region to be either preexisting (Low and Zhang, 2002) or formed during eruption (Gosling et al., 1995). The current paradigm is that the flux of the envelope field is transferred to the flux rope during the eruption, so at 1 AU only the flux rope is observed. If the envelope field continues to be present, one should be able to observe counterstreaming electrons in the sheath of shock-driving CMEs. There seems to be no evidence for such counterstreaming (Gosling 2004, private communication). This may be a good test to understand the interplanetary evolution of CMEs. Another kind of evolution is the change in topology of the CME field lines from closed to open via interchange reconnection process (Larson et al., 1997; Crooker et al., 2002), which might explain the magnetic flux balance in the heliosphere. While important, such reconnection between background solar wind and the ICME field lines does not appear to be able to destroy the overall ICME structure over distances of 1 AU (Schmidt and Cargill, 2003). More studies are needed to assess

how common such evolution is, given the fact that magnetic clouds are observed throughout the heliosphere (Burlaga et al., 1993).

12. Summary

CMEs are multithermal structures in general, carrying coronal (∼2 MK) material in the front followed by cool prominence (∼8000 K) material in some cases and hot flare-material (∼10 MK) in others. In some CMEs, there is a void between the frontal structure and the prominence core, with coronal temperature and a magnetic field stronger than in the ambient corona. The prominence core can be observed in X-rays, microwaves, H-alpha, and EUV as hot ejecta (thermal emission) or as a moving type IV burst due to nonthermal electrons trapped in the ejecta. After the eruption, hot post-eruption arcades or flare loops form, marking the location of eruption on the Sun. CME speeds vary over three orders of magnitude, from $\sim$ 20 km s^{-1} to more than 2500 km s^{-1} and the average speed shows a clear increase towards the solar activity maximum. Typical CMEs are $\sim 47^{\circ}$ wide, but a small fraction of fast and wide CMEs have far-reaching heliospheric consequences. Fast CMEs drive powerful fast mode shocks, which in turn accelerate electrons and ions over extended periods of time. All the CME substructures are likely to propagate into the heliosphere, producing various observational signatures. The shock-accelerated electrons produce type II radio bursts in the IP medium. While the protons and heavier ions accelerated by the shock near the Sun reach 1 AU in a few tens of minutes, locally accelerated energetic particles arrive with the shocks on the time scale of days. CMEs undergo varying acceleration due to a combination of propelling and retarding forces. Far from the Sun, most CMEs tend towards the speed of the solar wind and the magnitude of acceleration is several m s^{-2}. CMEs arriving at Earth can also cause major geomagnetic storms if they possess southward magnetic field component that can reconnect with Earth's magnetic field. These storms are associated with a number of phenomena in other layers of Earth's atmosphere and on the ground. A fraction of the CMEs observed near the Sun can propagate to the far reaches of the heliosphere and become part of the merged interaction regions of various scales. These CMEs also can scatter off galactic cosmic rays, probably contributing to the 22-year modulation cycle.

The superior capability of the SOHO/LASCO coronagraphs enabled us to observe CMEs with unprecedented continuity and spatial coverage and hence we have a better picture of the whole phenomenon over a significant fraction of solar cycle 23, and we hope that SOHO will

acquire data over the remaining part of the solar cycle. The solar maximum CME rate was found to be much higher than previously thought. Even though there is good correlation between CME rate and Sunspot number, their peaks were nearly two years apart. To fully understand this relationship, we need to consider both sunspot (active region) and non-spot (filament region) sources of CMEs. High-latitude CMEs associated with polar crown filaments and low-latitude CMEs from the active region belt naturally form into two groups, which have wider implications than just the initiation issue. The cessation of high-latitude activity seems to clearly mark the completion of polarity reversals at least for cycles 23 and 21. This leads to an important conclusion that the polarity reversal is an energetic process involving the release of large amounts of energy. The rate of high latitude CMEs is clearly related to the migration of closed field structures to the poles (one indication is the rush to the poles of the polar crown filaments as signified by the high tilt angles.) Occasionally, the high-latitude rate can be as high as the low-latitude rate, but overall the low-latitude activity dominates.

Halo CMEs and fast-and-wide CMEs are important from the space weather point of view. These CMEs constitute a small subset of all CMEs and can be studied independent of the thousands of ordinary CMEs. We need to focus on front-sided halo CMEs for assessing their geoeffectiveness. The shock-driving capability of the fast and wide CMEs is an important aspect consistent with the current paradigm that energetic particles (in large events) are accelerated by these shocks. The structural and magnetic connection between CMEs near the Sun and in the heliosphere is clear in a crude sense, but the details are still missing. The vast amount of CME data put out by SOHO and the availability of a wealth of complementary data from space and ground is likely to lead to appreciable progress in CME research. The birth, life, and death of CMEs involve an intriguing chain of physical processes on a grand scale, fully observable using ground and space borne instruments. Thus the study of CMEs is of enormous interest in uncovering the underlying physics of interaction between plasma and magnetic field. Studying CMEs is also crucial in understanding the space environment, into which humans often venture, because they cause intense geomagnetic storms and drive shocks that rise the particle radiations to hazardous levels.

Acknowledgments: I thank L. Burlaga, H. Hudson, S. Kahler, A. Ciaravella, S. T. Suess, and O. C. St. Cyr for critical comments on the manuscript. I thank S. Yashiro and A. Lara for help with some of the figures, and S. Nunes for cross-checking the references. I acknowledge the LASCO team headed by R. A. Howard and the Wind/WAVES team headed by J.-L. Bougeret and M. L. Kaiser for making their data avail-

able on line. SOHO is a project of international cooperation between ESA and NASA.

References

Andrews, M. & Howard, R. A., 2001, Space Sci. Rev., 95, 127
Antiochos, S. K., Dahlburg, R. B., & Klimchuk, J. A., 1999, Astrophys. J., 510, 485
Anzer, U. & Pnueman, G. W., 1982, Solar Phys., 17, 129.
Balogh, A., 2002, The evolving Sun and its influence on Planetary Environments, ed. B. Montosinos, A. Gimenez. & E.F. Guinan, ASP Conf. Ser., 269, 37
Barghouty, A. F. & Mewaldt, R. A., 2000, AIP Conf. Proc. 528: Acceleration and Transport of Energetic Particles Observed in the Heliosphere, 528, p. 71
Bastian, T. S., Pick, M., Kerdraon, A., Maia, D., & Vourlidas, A., 2001, Astrophys. J., 558, L65
Bhatnagar, A., 1996, Astrophys. Space Sci., 243, 105
Bieber, J. et al., 1999, Phys. Rev. Lett., 83, 674
Bieber, J. et al., 2002, Astrophys. J., 567, 622
Bilenko, I. A., 2002, Astron. Astrophys, 396, 657
Boischot, A., 1957, Comptes Rendus Acad. Sci., Paris, 244, 1326
Borrini, G., Gosling, J. T., Bame, S. J., & Feldman, W. C., 1982, J. Geophys. Res., 87, 4365
Bothmer, V., & Rust, R. M., 1997, Coronal Mass Ejections, ed. N. Crooker, J. Joselyn, & J. Feynman (Washington DC: Amer. Geophys. Union), p. 139
Bothmer, V. & Schwenn, R., 1994, Space Sci. Rev., 70, 215
Bougeret, J.-L., et al., 1995, Space Sci. Rev., 71, 231
Brueckner, G. E. et al., 1995, Solar Phys., 162, 357
Burkepile, J. et al., 2002, Fall AGU Meeting 2002, abstract #SH21A-0
Burlaga, L., Sittler, E., Mariani, F., & Schwenn, R., 1981, J. Geophys. Res., 86, 6673
Burlaga, L. et al ., 1982, Geophys. Res. Lett., 9, 1317
Burlaga, L. F., Goldstein, M. L., McDonald, F. B., & Lazarus, A. J., 1985, J. Geophys. Res., 90, 12027
Burlaga, L., Behannon, K. W. & Klein, L. W, 1987, J. Geophys. Res., 92, 5725
Burlaga, L. F., McDonald, F. B., & Ness, N. F., 1993, J. Geophys. Res., 98, 1
Burlaga, L. et al., 1998, J. Geophys. Res., 103, 277
Cane, H., 1983, JPL Solar Wind Five, p. 703.

Cane, H., Sheeley, N. R., & Howard, R. A., 1987, J. Geophys. Res., 92, 9869
Cane, H. & Richardson, I. G., 2003, J. Geophys. Res., 108(4), SSH 6-1
Cargill, P. J., Chen, J., Spicer, D. S., & Zalesak, S. T., 1996, J. Geophys. Res., 101, 4855
Chen, J., 1989, Astrophys. J., 338, 453
Chen, J. et al., 2000, Astrophys. J., 533, 481
Chen, J. & Krall, J., 2003, J. Geophys. Res., 108, A11, 1410
Chen, P. F. & Shibata, K., 2000, Astrophys. J., 545, 524
Chertok, I. M., Grechnev, V. V., Hudson, H. S., & Nitta, N. V., 2004, J. Geophysical Res., 109, 2112
Ciaravella, A. et al., 2003, Astrophys. J., 597, 1118
Cliver, E. W., 1996, High Energy Solar Physics, ed. R. Ramaty, N. Mandzhavidze, & X.-M. Hua, AIP Conf. Proc., Vol. 374. Woodbury, NY, p.45
Cliver, E. W., & Ling, A. G., 2001a, Astrophys. J., 551, L189
Cliver, E. W., & Ling, A. G., 2001b, Astrophys. J., 556, 432
Cliver, E. W., St. Cyr, O. C., Howard, R. A., & McIntosh, P. S., 1994, in Solar coronal structures, ed. V. Rusin, P. Heinzel & J.-C. Vial, VEDA Publishing House of the Slovak Academy of Sciences, p.83
Cliver, E. W., Webb, D.F. & Howard, R. A., 1999, Solar Phys., 187, 89
Cliver, E. W., Ling, A. G. & Richardson, I. G., 2003, Astrophys. J., 592, 574
Crifo, F., Picat, J. P., & Cailloux, M., 1983, Solar Phys., 83, 143
Crooker, N. U., 2000, JASTP, 62, 1071
Crooker, N. U., Gosling, J. T., & Kahler, S. W., 2002, J. Geophys. Res., 107(A2), SSH 3-1
DeMastus, H. L., Wagner, W. J., & Robinson, R. D., 1973, Solar Phys., 31, 449
Delaboudiniere, J.-P. et al., 1995, Solar Phys., 162, 291
Desai, M. et al., 2003, Astrophys. J., 588, 1149
Dulk, G. A., & McLean, D. J., 1978, Solar Phys., 57, 279
Dryer, M., 1996, Solar Phys., 169, 421
Eddy, J. A., 1974, Astron. Astrophys., 34, 235
Engvold, O., 1997, in New Perspectives on Solar Prominences (IAU Colloquium 167), ed. D. Rust, D. F. Webb, & B. Schmieder, Vol. 150, p. 23
Feynman, J. & S. F. Martin, 1995, J. Geophys. Res., 100, 3355
Filippov, B. P. 1998, in New Perspectives on Solar Prominences (IAU Colloquium 167), ed. D. Rust, D. F. Webb, & B. Schmieder, Vol. 150, p. 342
Forbes, T., 2000, J. Geophys. Res., 105, 23153

Forbes, T. G., P. A. Isenberg, & E. R. Priest, 1994, Solar Phys., 150, 245

Funsten, H. O. et al., 1999, J. Geophys. Res., 104, 6679

Gary, D. et al., 1984, Astron. Astrophys., 134, 222

Gold, T, 1955, J. Geophys. Res., 64, 1665

Gopalswamy, N. 1999, Solar Physics from Radio Observations, Eds.: T. S. Bastian, N. Gopalswamy & K.Shibasaki, NRO Report No. 479., p.141

Gopalswamy, N., 2002, Solar-Terrestrial Magnetic Activity and Space Enviroment, COSPAR Colloquia Series, Vol. 14, edited by H. N. Wang & R. L. Xu, p. 157

Gopalswamy, N., 2003a, Geophys. Res. Lett., 30(12), SEP 1-1

Gopalswamy, N., 2003b, Adv. Space Research, 31(4), 869

Gopalswamy, N. & Kundu, M. R., 1989, Solar Phys., 122, 145

Gopalswamy, N. & Kundu, M. R., 1992, Particle acceleration in cosmic plasmas, AIPC 264, p. 257

Gopalswamy, N. & Kundu, M. R., 1993, Solar Phys., 143, 327

Gopalswamy, N., Kundu, M. R., Hanaoka, Y., Enome, S., & Lemen, J. R. 1996, New Astronomy, 1, 207

Gopalswamy, N. et al., 1997a, Astrophy. J., 475, 348

Gopalswamy, N. et al., 1997b, Astrophy. J., 486, 1036

Gopalswamy, N., & Hanaoka, Y, 1998, Astrophy. J., 498, L179.

Gopalswamy, N. et al., 1998, Geophys. Res. Lett., 25, 2485

Gopalswamy, N., Yashiro, S., Kaiser, M. L., Thompson, B. J., & Plunkett, S., 1999, Solar Physics with Radio Observations, Eds.: T. S. Bastian, N. Gopalswamy & K. Shibasaki, NRO Report No. 479., p.207

Gopalswamy, N. & Thompson, B. J., 2000, JASTP, 62, 1457

Gopalswamy, N. et al., 2000a, Geophys. Res. Lett., 27, 145

Gopalswamy, N. et al., 2000b, Geophys. Res. Lett., 27, 1427

Gopalswamy, N. Hanaoka, Y. & Hudson, , 2000c Adv. Space Res., 25(9), 1851

Gopalswamy, N., Kaiser, M. L., Sato, J., & Pick, M., 2000d, in High Energy Solar Physics, Ed. R. Ramaty & N. Mandzhavidze, PASP Conf Ser., vol. 206, p. 355

Gopalswamy, N., Lara, A., Kaiser, M. L., & Bougeret, J.-L., 2001a, J. Geophys. Res., 106, 25261

Gopalswamy, N., Lara, A., Yashiro, S., Kaiser, M. L. & Howard, R. A., 2001b, J. Geophys. Res., 106, 29107

Gopalswamy, N., Yashiro, S., Kaiser, M. L., Howard, R. A., & Bougeret, J.-L., 2001c, Astrophys. J., 548, L91

Gopalswamy, N., St. Cyr, O. C., Kaiser, M. L., Yashiro, S., 2001d, Solar Phys., 203, 149

Gopalswamy, N., Yashiro, S., Kaiser, M. L., Howard, R. A. & Bougeret, J.-L., 2001e, J. Geophys. Res., 106, 29,219
Gopalswamy, N. & Kaiser, M. L., 2002, Adv. Space Res., 29(3), 307
Gopalswamy, N., Yashiro, S., Kaiser, M. L., Howard, R. A., & Bougeret, J.-L., 2002a, Geophys. Res. Lett., 29(8), DOI:10.1029/2001GL013606
Gopalswamy, N., et al., 2002b, Astrophys. J., 572, L103
Gopalswamy, N. Shimojo, M., Lu, W., Yashiro, S., Shibasaki, K. & Howard, R. A., 2003a, Astrophys. J., 586, 562
Gopalswamy, N., Lara, A., Yashiro, S., Nunes, S., & Howard, R. A., 2003b, Solar variability as an input to the Earth's environment, Ed.: A. Wilson. ESA SP-535, Noordwijk: ESA Publications Division, p. 403
Gopalswamy, N. et al., 2003c, Geophys. Res. Lett., 30(12), SEP 3-1
Gopalswamy, N., Manoharan, P. K., & Yashiro, S., 2003d, Geophys. Res. Lett., 30(24), SSC 1-1
Gopalswamy, N., Lara, A., Yashiro, S., & Howard, R. A., 2003e, Astrophys. J., 598, L63
Gosling, J. T., 1993, J. Geophys. Res., 98, 18937
Gosling, J. T., 1997, Coronal Mass Ejections, ed. N. Crooker, J. Joselyn, & J. Feynman (Washington DC: Amer. Geophys. Union), p. 9
Gosling, J. T., Asbridge, J. R., Bame, S. J., Hundhausen, A. J., & Strong, I. B., 1968, J. Geophys. Res., 73, 43
Gosling J. T. et al., 1974, J. Geophys. Res., 79, 4581
Gosling, J. T. et al., 1976, Solar Phys., 48, 389
Gosling, J. T., Bame, S. J., McComas, D. J., & Phillips, J. L., 1990, Geophys. Res. Lett., 17, 901
Gosling, J. T., McComas, D. J., Phillips, J. L., & Bame, S. J., 1992, J. Geophys. Res., 97, 6531
Gosling, J. T. et al., 1994, Geophys. Res. Lett., 21, 2271
Gosling, J. T., Birn, J., & Hesse, M., 1995, Geophys. Res. Lett., 22, 869
Gosling, J. T. & Forsyth, R. J., 2001, Space Sci. Rev., 97, 87
Hanaoka et al., 1994, PASJ, 46, 205
Hansen, R. T., Garcia, C. J., Grognard, R. J.-M., & Sheridan, K. V., 1971, Proc. ASA, 2, 57
Harrison, R. A., 1990, Solar Phys., 126, 185
Harrison, R. A., 1991, Adv. Space res., 11(1), 25
Harrison, R. A., 1995, Astron. Astrophys., 304, 585
Harvey, K. & Recely, F., 2002, Solar Phys., 211, 31
Henke, T., 1998, Geophys. Res. Lett., 25, 3465
Hewish, A., Tappin, S. J. & Gapper, G. R., 1985, Nature, 314, 137
Hildner, E. et al., 1976, Solar Phys., 48, 127

Hildner, E., 1977, Study of Travelling Interplanetary Phenomena, ed. M.A. Shea, D.F. Smart, & S.T. Wu., ASSL, Vol. 71, p.3
Hirshberg, J., Bame, S. J., & Robbins, D. E., 1972, Solar Phys., 23, 467.
Holman, G. D. & Pesses, M. E., 1983, Astrophys. J., 267, 837
Hori, K. & Culhane, J. L., 2002, Astron. Astrophys., 382, 666.
House, L. L., Wagner, W. J., Hildner, E., Sawyer, C., & Schmidt, H. U. 1981, Astrophys. J., 244, L117
Howard, R. A., Michels, D. J., Sheeley, N. R., Jr., & Koomen, M. J., 1982, Astrophys. J., 263, L101
Howard, R. A., Sheeley, N. R., Jr., Michels, D. J., & Koomen, M. J., 1984, Adv. Space Res., 4(7), 307
Howard, R. A., Michels, D., Sheeley, N. R., & Koomen, M. J., 1985, J. Geophys. Res., 90, 8173
Howard, R. A., Michels, D., Sheeley, N. R., & Koomen, M. J., 1986, ASSL Vol. 123: The Sun and the Heliosphere in Three Dimensions, ed. R. Marsden, D. Reidel, Norwell, Mass., p. 107
Howard, R. A. et al., 1997, Coronal Mass Ejections, ed. N. Crooker, J. Joselyn, & J. Feynman (Washington DC: Amer. Geophys. Union), 17
Hudson, H., 1999, Eds.: T. S. Bastian, N. Gopalswamy & K. Shibasaki, NRO Report No. 479, p.15
Hudson, H. & D. F. Webb, 1997, in Coronal Mass Ejections, ed. N. Crooker, J. A. Joselyn, & J. Feynman, AGU Monograph 99, p. 27
Hudson, H., Acton, L. W. & Freeland, S. L., 1996, Astrophys. J., 470, 629
Hudson, H. S. & Cliver, E. W., 2001, J. Geophys. Res., 106, 25199
Hudson, H. S., Kosugi, T., Nitta, N. V., & Shimojo, M., 2001, Astrophys. J., 561, L211
Hudson, H. S., Khan, J. I., Lemen, J. R., Nitta, N. V., & Uchida, Y., 2003, Solar phys., 212, 121
Hundhausen, A. J. 1987, Proc. Sixth international Solar Wind Conference, Vol. 1, ed. V. J. Pizzo, T. E. Holzer, & D. G. Sime, High Altitude Observatory, NCAR, Boulder, Colorado, p. 181
Hundhausen, A. J., 1993, J. Geophys. Res., 98, 13,177
Hundhausen, A. J., 1997, in Coronal Mass Ejections, ed. N. Crooker, J. A. Joselyn, & J. Feynman, AGU Monograph 99, p. 1
Hundhausen, A. J., 1999, Many Faces of the Sun, ed. K. T. Strong, J. L. R. Saba, & B. M. Haisch, Springer-Verlag, New York, p. 143
Hundhausen, A., Bame, S. J., & Montgomery, M. D., 1970, J. Geophys. Res., 75, 4631
Illing, R. M. E. & Athay, G., 1986, Solar Phys., 105, 173
Jackson, B., 1985, Solar Phys., 100, 563
Jackson, B. & Howard, R. A., 1993, Solar Phys., 148, 359

Jokipii, J. R., Levy, E. H., & Hubbard, W. B., 1977, Astrophys. J., 213, 861
Kahler, S. W., 1992, ARA&A, 30, 113
Kahler, S. W., 1993, J. Geophys. Res., 98, 5607
Kahler, S. W., 1994, Astrophys. J., 428, 837
Kahler, S. W., 2001, J. Geophys. Res., 106, 20947
Kahler, S. W.,Hildner, E. & van Hollebeke, M. A. I., 1978, Solar Phys., 57, 429
Kahler, S. W., Sheeley, N. R., Howard, R. A., Michels, D. J., & Koomen, M. J., 1984, Solar Phys., 93, 133
Kahler, S. W., et al., 1985, J. Geophys. Res., 90, 177
Kahler, S. W., 1987, Sixth International Solar Wind Conference, Ed. V.J. Pizzo, T. Holzer, & D.G. Sime, NCAR Technical Note NCAR/TN-306+Proc, Volume 2, 1987., p.215
Kahler, S. W., Sheeley, N. R., Jr. & Liggett, M., 1989, Astrophys. J., 344, 1026
Kallenrode, M.-B., & Cliver, E. W., 2001, Proc. ICRC 2001, 3319
Kim, I. & Alexeyeva, V., 1994, Solar Active region Evolution: Comparing Models with Observations, ed. K. S. Balasubramaniam & G. Simon, ASP Conf. ser. 68, p. 403
Klassen, A., H. Aurass, G. Mann & B. J. Thompson, 2000, Astron. Astrophys. (Sup.), 141, 357.
Klein, L. W. & Burlaga, L. F., 1982, J. Geophys. Res., 87, 613
Klimchuk, J. A., 2000, Space Weather, ed. P. Song, H. J. Singer, & G. L. Sisco, AGU Monograph 125, p. 143
Klimchuk, J. A., et al., 1994, in X-Ray Solar Physics from Yohkoh, ed. Y. Uchida (Tokyo: Universal Academy Press), 181
Kocharov, L. & Torsti, J., 2002, Solar Phys., 207, 149
Kohl, J. L. et al., 1995, Solar Phys., 162, 313
Lara, A., Gopalswamy, N., Nunes, S., Muñoz, G., & Yashiro, S., 2003, Geophys. Res. Lett., 30, No.12, SEP 4-1
Lara, A., Gopalswamy, N., Caballero-Lopez, R. A., Yashiro, S. & Valdes-Galicia, J. F., 2004, Astrophys. J. (submitted)
Larson, D. E. et al., 1997, Geophys. Res. Lett., 24, 1911
Lee, M., 1997, in Coronal Mass Ejections, ed. N. Crooker, J. A. Joselyn, & J. Feynman, AGU Monograph 99, p. 227
Lepping, R. L., J. A. Jones, & L. F. Burlaga, 1990, J. Geophys. Res., 95, 11957
Lepri, S. et al., 2001, J. Geophys. Res., 106, 29231
Lin, R. P., 1987, Solar Phys., 113, 217
Lindemann, F. A., 1919, Phil. Mag., 38, 669

Lindsay, G. M., Luhmann, J. G., Russell, C. T., & Gosling, J. T., 1999, J. Geophys. Res., 104, 12515

Linker, J. A., Lionello, R., Mikić, Z., & Amari, T., 2001, J. Geophys. Res., 106, 25165

Lorenc, M., Pasorek, L., & Rybanský, M., 2003, in Solar Variability as an input to the Earth's Environment, ESA-SP, 535, Noordwijk: ESA Publications Division, p. 129

Low, B. C., 1996, Solar Phys., 167, 217

Low, B. C. 1997, in Coronal Mass Ejections, ed. N. Crooker, J. A. Joselyn, & J. Feynman, AGU Monograph 99, p. 39

Low, B. C., 2001, J. Geophys. Res., , 106, 25141

Low, B. C. & Zhang, M., 2002, Astrophys. J., 564, L53

Machado, M. et al., Astrophys. J., 326, 425

MacQueen, R. M. & R. Fisher, 1983, Solar Phys., 89, 89

MacQueen, R. M. et al., 1974, Astrophys. J., 187, L85

MacQueen, R. M. et al., 1980, Solar Phys., 65, 91

Magara, T. & Longcope, D. W., 2001, Astrophys. J., 559, L55

Makarov, V. I., Tlatov, A. G., & Sivaraman, K. R., 2001, Solar Phys., 202, 11

Malitson, H. H., Fainberg, J., & Stone, R. G., 1973, Astrophys. Lett., 14, 111

Mancuso, S. & Raymond, J. C., 2004, Astron. Astrophys., 413, 363

Mann, G., Klassen, A., Estel, C., & Thompson, B. J., 1999, in Proc. of 8th SOHO Workshop, Edited by J.-C. Vial & B. Kaldeich-Schmann., p.477

Manoharan, P. K., Gopalswamy, N., Lara, A. & Yashiro, S., 2004, J Geophys. Res., in press.

Martin, S. F. & McAllister, A. H., 1997, Coronal Mass Ejections, ed. N. Crooker, J. Joselyn, & J. Feynman (Washington DC: Amer. Geophys. Union), p. 127

Marubashi, K., 1997, Coronal Mass Ejections, ed. N. Crooker, J. Joselyn, & J. Feynman (Washington DC: Amer. Geophys. Union), p. 147

Mason, G. M., Mazur, J. E., & Dwyer, J. R., 1999, Astrophys. J., 525, L133

Michalek, G., Gopalswamy, N. & Yashiro, S., 2003, Astrophys. J., 584, 472

Michels, D. J., Howard, R. A., Koomen, M. J., & Sheeley, N. R., Jr., 1980, Radio physics of the sun, ed. M.R. Kundu & T. E. Gergely, Dordrecht, D. Reidel, p.439

Moon, Y.-J. et al., 2002, Astrophys. J., 581, 94

Moore, R. L., Falconer, D. A., Porter, J. G., & Suess, S. T. 1999, Astrophys. J., 526, 505

Moore, R. L., Sterling, A. C., Hudson, H. S., & Lemen, J. R. 2001, Astrophys. J., 552, 833
Moreton, G. E., 1960, Astron. J., 65, 494
Mullan, D. J., 1997, AIP Conf. Proc. 385: Robotic Exploration Close to the Sun: Scientific Basis, 385, 235
Mulligan, T., Russell, R. T., & Luhmann, J., 1998, Geophys. Res. Lett., 25, 2959
Munro, R. H. et al. 1979, Solar Phys. 61, 201
Newkirk, G., Hundhausen, A. J. & Pizzo, V., 1981, J. Geophys. Res., 86, 5387
Narukage, N., Hudson, H. S., Morimoto, T., Akiyama, S., Kitai, R., Kurokawa, H., & Shibata, K., 2002, Astrophys. J., 572, L109
Nuegebauer, M. & Goldstein, B. E., 1997, in Coronal Mass Ejections, ed. N. Crooker, J. A. Joselyn, & J. Feynman, AGU Monograph 99, p.
Nitta, N. & Akiyama, S. 1999, Astrophys. J., 525, L57
Nitta, N. V. & Hudson, H. S., 2001, Geophys. Res. Lett., 28, 3801
Obayashi, T., 1962, J. Geophys. Res., 67, 1717
Pallavicini, R.; Serio, S.; Vaiana, G. S., 1977, Astrophys. J.,216, 108
Park, Y. D., Moon, Y.-J., Kim, I., & Yun, H. S. 2002, Ap&SS, 279, 343
Payne-Scott, R., Yabsley D. E., & Bolton, J. G., 1947, Nature, 160, 256
Plunkett, S. P. et al., 2000, Solar Phys., 61, 201
Potgeiter, M. S., Burger, R. A., & Ferreira, S. E. S., 2001, Space Sci. Rev., 97, 295
Poland, A., Howard, R. A., Koomen, M. J., Michels, D. J., Sheeley, N. R., Jr., 1981, Solar phys., 69, 169
Ramesh, R., Kathiravan, C., & Sastry, C. V., 2003, Astrophys. J., 591, L163
Raymond, J. et al., 2000, Geophys. Res. Lett., 27, 1439
Reames, D. V., 1999, Space Sci. Rev., 90, 413
Reames, D. V., 2001, Geophysical Monograph 125, AGU, Washington DC, 101
Reames, D. V., Ng, C. K., & Tylka, A. J., 1999, Geophys. Res. Lett., 26, 3585
Reiner, M. J. & Kaiser, M. L., 1999, JGR, 104, 16979
Reiner, M. J. et al., 2001, JGR, 106, 25279
Reisenfeld, D. B., Gosling, J. T., Forsyth, R. J., Riley, P., & St. Cyr, O. C., 2003, Geophys. Res. Lett., 30, 5
Robinson, R. D., 1985, Solar Phys., 95, 343
Robinson, R. D. & Stewart, R. T., 1985, Solar Phys., 97, 145
Rusin, V. & Rybansky, M., 1983, BAICz, 34, 25
Rust, D. M. & Hildner, E., 1976, Solar Phys., 48, 381
Saito, K. & Tandberg-Hanssen, E., 1973, Solar Phys., 31, 105

Schmidt, J. M. & Cargill, P. J. 2003, J. Geophysical Res., 108, SSH 5-1
Schwenn, R., 1986, Space Sci. Rev., 44, 139
Schwenn, R., 1996, Astrophys. Space Sci., 243, 187
Sheeley, N., Howard, R. A., Koomen, M. J., & Michels, D. J., 1983, Astrophys. J., 272, 349
Sheeley, N. R. et al., 1984, Astrophys. J., 279, 839
Sheeley, N. R., et al., 1985, J. Geophys. Res., 90, 163
Sheeley, N. R., J. H. Walters, Y.-M. Wang, & R. A. Howard, 1999, J. Geophys. Res., 104, 24739
Sheeley, N. R., Hakala, W. N., Wang, Y.-M., 2000, J. Geophys. Res., 105, 5081
Shibata, K., et al., 1992, PASJ, 44, 173
Shibata, K., et al., 1995, ApJ, 451, L83
Sonett, C. P., Colburn, C. D. S., Davis, L., Smith, E. J., & Coleman, P. J., 1964, Phys. Rev. Lett., 13, 153
St. Cyr, O. C. & Webb, D. F., 1991, Solar Phys., 136, 379
St. Cyr, O. C., Burkepile, J. T., Hundhausen, A. J., & Lecinski, A. R., 1999, J. Geophys. Res. , 104, 12493
St. Cyr, O. C. et al., 2000, J. Geophys. Res., 105, 18169
Steinolfson, R. S., 1992, Proc. Of the 26th ESLAB Symposium on the Study of the Solar-terrestrial physics
Sterling, A., 2003, Solar variability as an input to the Earth's environment, Ed.: A. Wilson, ESA SP-535, Noordwijk: ESA Publications Division, p. 415
Sterling, A., & Hudson, H., 1997, Astrophys. J., 491, L55
Stewart, R. T., 1985, Solar Radiophysics, Cambridge and New York, Cambridge, University Press, p. 361
Tandberg-Hanssen, E. 1995, The Nature of Solar Prominences, Kluwer, Dordrecht
Tappin, S. J. & Simnett, G. M. 1997, Correlated Phenomena at the Sun, in the Heliosphere and in Geospace, Edited by A. Wilson. European Space Agency, ESA SP-415, p.117
Thompson, B. J. et al., 1999, Astrophys. J., 517, L151
Tokumaru, M., Kojima, M., Fujiki, K., & Yokobe, A., 2000, J. Geophys. Res., 105, 10,435
Tousey, R., 1973, The solar corona, Space Res., 13, 713
Tousey, R., Howard, R. A., & Koomen, M. J., 1974, Bull. American Astron. Soc., 6, 295
Tylka, A., 2001, J. Geophys. Res., 106, 25,233
Uchida, Y., 1960, PASJ, 12, 376
Venkatakrishnan, P. V. & Ravindra, B., 2003, Geophys. Res. Lett., 30(23), SSC 2-1

Vourlidas, A., Buzasi, D., Howard, R. A., & Esfandiari, E., 2002, Solar variability: from core to outer frontiers, Ed. A. Wilson. ESA SP-506, Vol. 1. Noordwijk: ESA Publications Division, p. 91

Vourlidas, A., Wu, S. T., Wang, A. H., Subramanian, P., & Howard, R. A, 2003, Astrophys. J., 598, 1392

Wagner, W. J., 1984, ARA&A, 22, 267

Wagner, W. J. et al., 1981, Astrophys. J., 244, L123

Wagner, W. J. & MacQueen, R. M., 1983, Astron. Astrophys., 120, 136

Wang, Y.-M., Sheeley, N. R., & Andrews, M. D., 2002, J. Geophys. Res., 10

Webb, D. F., 2002, Half a Solar Cycle with SOHO, ed. A. Wilson, ESA SP-508, Noordwijk: ESA Publications, p. 409

Webb, D. F., Krieger, A. S. & Rust, D. M., 1976, Solar phys., 48,159.

Webb, D. F., E. W. Cliver, N. U. Crooker, O. C. St. Cyr, & B. J. Thompson, J. Geophys. Res., 105, 7491, 2000.

Webb, D. F., Davis, J. M. & McIntosh P. S., 1984, Solar Phys., 92, 109

Webb, D. F., Nolte, J. T., Solodyna, C. V. & McIntosh, P., 1978, Solar Phys., 58, 389

Webb, D. F. & Hundhausen, A. J. 1987, Solar Phys., 108, 383.

Webb, D. F., & Howard, R. A., 1994, J. Geophys. Res., 99, 4201

Webb, D. F., Cliver, E. W., Crooker, N. U., St. Cyr, O. C., & Thompson, B. J., 2000, J. Geophys. Res., 105, 7491

Whang, Y.-C., 1987, J. Geophys. Res., 92, 4349

White, S. M., Kundu, M. R. & Gopalswamy, N., 1991, Astrophys. J., 366, L43

Wild, J. P., 1950, Aust. J. Sci. Ser. A, 3, 541

Wilson, R. M., & E. Hildner, 1984, Sol. phys., 91, 169

Wood, B. E. et al., 1999, Astrophys. J., 512, 484

Wu, S. T., Guo, W. P., Plunkett, S. P., Schmieder, B., & Simnett, G. M., 2000, JATP, 62, 1489

Wu, S. T., Wang, A. H., & Gopalswamy, N, 2002, in SOLMAG 2002, Ed. H. Sawaya-Lacoste, ESA SP-505. Noordwijk, Netherlands, p. 227

Yashiro, S., Gopalswamy, N., Michalek, G., & Howard, R. A., 2003, Adv. Space Res., 32, 2631

Yashiro, S. et al., 2004, J. Geophys. Res., in press

Yeh, T, A dynamical model of magnetic clouds, Asrophys. J., 438, 975, 1995

Zhang, M. & Low, B. C., 2001, Asrophys. J., 561, 406

Zhang, J., Dere, K. P., Howard, R. A., Kundu, M. R., White, S. M., 2001, Asrophys. J., 559, 452